# Urban influence on the concentration and composition of submicron particulate matter in central Amazonia

Suzane S. de Sá (1), Brett B. Palm (2), Pedro Campuzano-Jost (2), Douglas A. Day (2), Weiwei Hu (2), Gabriel Isaacman-VanWertz[a] (3), Lindsay D. Yee (3), Joel Brito[b] (4), Samara Carbone[c] (4), Igor O. Ribeiro (5), Glauber G. Cirino[d] (6), Yingjun J. Liu[e] (1), Ryan Thalman[f] (7), Arthur Sedlacek (7), Aaron Funk (8), Courtney Schumacher (8), John E. Shilling (9), Johannes Schneider (10), Paulo Artaxo (4), Allen H. Goldstein (3), Rodrigo A.F. Souza (5), Jian Wang (7), Karena A. McKinney[g] (1), Henrique Barbosa (4), M. Lizabeth Alexander (11), Jose L. Jimenez (2), Scot T. Martin[*] (1, 12)

(1) School of Engineering and Applied Sciences, Harvard University, Cambridge, Massachusetts, USA
(2) Department of Chemistry and Cooperative Institute for Research in Environmental Sciences, University of Colorado, Boulder, Colorado, USA
(3) Department of Environmental Science, Policy, and Management, University of California, Berkeley, California, USA
(4) Institute of Physics, University of São Paulo, São Paulo, Brazil
(5) School of Technology, Amazonas State University, Manaus, Amazonas, Brazil
(6) National Institute for Amazonian Research, Manaus, Amazonas, Brazil
(7) Brookhaven National Laboratory, Upton, New York, USA
(8) Department of Atmospheric Sciences, Texas A&M University, College Station, Texas, USA
(9) Atmospheric Sciences and Global Change Division, Pacific Northwest National Laboratory, Richland, WA, USA
(10) Particle Chemistry Department, Max Planck Institute for Chemistry, Mainz, Germany
(11) Environmental Molecular Sciences Laboratory, Pacific Northwest National Laboratory, Richland, Washington, USA
(12) Department of Earth and Planetary Sciences, Harvard University, Cambridge, Massachusetts, USA
[a] Now at Department of Civil and Environmental Engineering, Virginia Tech, Blacksburg, Virginia, USA
[b] Now at Laboratory for Meteorological Physics (LaMP), University Blaise Pascal, Aubière, France
[c] Now at Federal University of Uberlândia, Uberlândia, Minas Gerais, Brazil
[d] Now at Department of Meteorology, Geosciences Institute, Federal University of Pará, Belém, Brazil
[e] Now at University of California, Berkeley, California, USA
[f] Now at Department of Chemistry, Snow College, Richfield, Utah, USA
[g] Now at Colby College, Waterville, Maine, USA

Submitted: February 2018

*Atmospheric Chemistry and Physics*

[*]To Whom Correspondence Should be Addressed

*E-mail: scot_martin@harvard.edu*

*https://martin.seas.harvard.edu/*

**Abstract**

Fundamental to quantifying the influence of human activities on climate and air quality is an understanding of how anthropogenic emissions affect the concentrations and composition of airborne particulate matter (PM). The central Amazon basin, especially around the city of Manaus, Brazil, has experienced rapid changes in the past decades due to ongoing urbanization. Herein, changes in the concentration and composition of submicron PM due to pollution downwind of the Manaus metropolitan region are reported as part of the GoAmazon2014/5 experiment. A high-resolution time-of-flight aerosol mass spectrometer (HR-ToF-AMS) and a suite of other gas- and particle-phase instruments were deployed at the "T3" research site, 70 km downwind of Manaus, during the wet season. At this site, organic components represented on average 79 ± 7% of the non-refractory $PM_1$ mass concentration, which was in the same range as several upwind sites. The organic $PM_1$ was, however, considerably more oxidized at T3 compared to upwind measurements. Positive-matrix factorization (PMF) was applied to the time series of organic mass spectra collected at the T3 site, yielding three factors representing secondary processes (73 ± 15% of total organic mass concentration) and three factors representing primary anthropogenic emissions (27 ± 15%). Fuzzy c-means clustering (FCM) was applied to the afternoon time series of concentrations of $NO_y$, ozone, total particle number, black carbon, and sulfate. Four clusters were identified and characterized by distinct airmass origins and particle compositions. Two clusters, Bkgd-1 and Bkgd-2, were associated with background conditions. Bkgd-1 appeared to represent near-field atmospheric PM production and oxidation of a day or less. Bkgd-2 appeared to represent material transported and oxidized for two or more days, often with out-of-basin contributions. Two other clusters, Pol-1 and Pol-2, represented the Manaus influence, one apparently associated with the northern region of Manaus and the other

with the southern region of the city. A composite of the PMF and FCM analyses provided insights into the anthropogenic effects on PM concentration and composition. The increase in mass concentration of submicron PM ranged from 25% to 200% under polluted compared to background conditions, including contributions from both primary and secondary PM. Furthermore, a comparison of PMF factor loadings for different clusters suggested a shift in the pathways of PM production under polluted conditions. Nitrogen oxides may have played a critical role in these shifts. Increased concentrations of nitrogen oxides can shift pathways of PM production from $HO_2$-dominant to NO-dominant as well as increase the concentrations of oxidants in the atmosphere. Consequently, the oxidation of biogenic and anthropogenic precursor gases as well as the oxidative processing of pre-existing atmospheric PM can be accelerated. The combined set of results demonstrates the susceptibility of atmospheric chemistry, air quality, and associated climate forcing to anthropogenic perturbations over tropical forests.

## 1. Introduction

Secondary organic material (SOM) constitutes a large fraction of the atmospheric particle burden (Hallquist et al., 2009; Jimenez et al., 2009) and therefore has important effects on the Earth's radiation balance, atmospheric visibility, and human health. SOM is a complex mixture of compounds resulting from many chemical pathways, and the processes underlying the production of SOM remain poorly understood. Models are especially challenged to accurately represent production of SOM in regions where there is a mix of biogenic and anthropogenic emissions (de Gouw et al., 2008; Glasius and Goldstein, 2016; Shrivastava et al., 2017). Possible shifts in the contributing mechanisms of SOM production between background and polluted conditions must be understood and quantified for distinct environments on the globe to test and enable accurate modeling predictions.

Several field observations, mainly in mid-latitudes of the Northern Hemisphere, and modeling efforts have suggested that the production of SOM from biogenic precursor compounds becomes more efficient in polluted air (Weber et al., 2007; Goldstein et al., 2009; Hoyle et al., 2011; Huang et al., 2014; Zhang et al., 2018). In the northeastern USA, de Gouw et al. (2005) showed that concentrations of organic particulate matter (PM) correlated well with anthropogenic tracers, yet the concentrations of the anthropogenic precursors were insufficient to explain the observed PM concentrations. In the southeastern USA, radioisotope analysis of organic PM determined that 70% to 80% of the carbon mass had a modern origin even as correlations were observed between SOM mass concentrations and anthropogenic VOC and CO concentrations (Weber et al., 2007). This finding and those of further field studies in the region together suggested that the organic PM was produced mainly from biogenic VOCs (BVOCs) yet modulated by anthropogenic emissions of $NO_x$ and $SO_2$ (Hu et al., 2015; Xu et al., 2015a; Xu et

al., 2015b; Zhang et al., 2018). In the western USA, ground and aircraft measurements observed the highest organic PM increases when air masses having high BVOC concentrations intercepted anthropogenic emissions (Setyan et al., 2012; Shilling et al., 2013). A metastudy for several locations in the USA concluded that air downwind of urban areas had increased organic PM concentrations due to the photochemical production of SOM (De Gouw and Jimenez, 2009). Models have estimated that 50% to 70% of the biogenic SOM mass concentration in several locations is modulated by anthropogenic emissions (Carlton et al., 2010; Heald et al., 2011; Spracklen et al., 2011). In addition, global-scale modeling studies have estimated an increase of 20% to 60% in the global annual mean SOM concentration relative to the pre-industrial period (Tsigaridis et al., 2006; Hoyle et al., 2009).

Many possible mechanisms may contribute to the effects of anthropogenic emissions on increased SOM production, including changes in gas-particle partitioning, new particle production and growth, and particle acidity. Changes in the concentrations of nitrogen oxides, however, should be regarded as a critical factor (Hoyle et al., 2011 and references therein). Different $NO_x$ regimes favor distinct gas-phase oxidation pathways, leading to different oxidation products and particle yields, as evidenced in isoprene photo-oxidation (Kroll et al., 2005, 2006; Hallquist et al., 2009; Worton et al., 2013; Liu et al., 2016b; Liu et al., 2016a). Isoprene accounts for half of global BVOC mass emissions, and tropical forests are responsible for about 80% of terpenoid emissions (Guenther et al., 2012). In the Amazon, isoprene is the dominant BVOC emitted by vegetation and is estimated to contribute to about half of the organic PM concentrations under background conditions (Kuhn et al., 2010; Chen et al., 2015; Yáñez-Serrano et al., 2015). Under $HO_2$-dominant conditions (i.e., low $NO_x$), isoprene epoxydiols (IEPOX) are produced in the gas phase and, through heterogenous reactions involving sulfate,

PM is produced (Paulot et al., 2009; Surratt et al., 2010). Depending on the relative importance of increased concentrations of sulfate and $NO_x$ associated with pollution in a given region, an enhancement or suppression of IEPOX-derived PM production relative to background conditions may occur (Xu et al., 2015a; de Sá et al., 2017). As part of GoAmazon2014/5, de Sá et al. (2017) demonstrated that PM derived from IEPOX generally decreased under polluted compared to background conditions downwind of Manaus. Nitrogen oxides in the pollution plume suppressed the production of isoprene hydroxyhydroperoxides (Liu et al., 2016b), leading to a decrease in the production of gas phase IEPOX and consequently of IEPOX-derived PM (de Sá et al., 2017).

Amazonia, the largest tropical forest in the world and a large global source of SOM, is comparatively understudied relative to northern mid-latitude regions, especially with respect to the influence of pollution on the SOM lifecycle (Martin et al., 2010a). Manaus, a city of over two million people in the central Amazon, continuously releases an urban plume into an otherwise mostly unperturbed region (Kuhn et al., 2010; Martin et al., 2017). The region downwind of Manaus, especially in the wet season in the absence of regional fires (Artaxo et al., 2013), offers a natural laboratory for the investigation of biogenic-anthropogenic interactions and the resulting consequences for the amount and composition of PM in the region..

The present study investigates the influences of urban pollution on the concentration and composition of fine particles in central Amazonia, focusing on organic PM and its several component classes. The analysis employs data sets collected in the wet season from February 1 to March 31, 2014, corresponding to the first Intensive Operating Period (IOP1) of the GoAmazon2014/5 experiment (Martin et al., 2016).A separate publication is planned for IOP2, corresponding to the dry season period of August 15 to October 15, when biomass burning emissions were prevalent (de Sá et al., in preparation). Herein, positive-matrix factorization

(PMF) of organic mass spectra measured by aerosol mass spectrometry (AMS) in conjunction with a clustering analysis of pollution indicators by Fuzzy c-means are employed to investigate the changes in particle concentration and composition associated with the influence of urban pollution downwind of Manaus.

## 2. Methodology

### 2.1 Site description

The primary site of this study, named "T3" (3.2133 °S, 60.5987 °W), was located 70 km to the west of Manaus, Brazil, in central Amazonia (Martin et al., 2016). The site was situated in a pasture of 2.5 km × 2 km surrounded by forest. Based on modeled flow trajectories of the pollution plume, the T3 site intercepted the plume about 40% of the time (Martin et al., 2017). Auxiliary sites "T0a" and "T0t", served as references for background conditions in relation to T3 (Figure S1). Site T0a (2.1466 °S, 59.0050 °W) refers to the Amazonian Tall Tower Observatory (ATTO; Andreae et al., 2015), located 150 km to the northeast of Manaus. Site T0t (2.5946°S, 60.2093°W) was situated 60 km to the north-northwest of Manaus in the Cuieiras Biological Reserve ("ZF2") and refers to tower "TT34", established in 2008 for the AMAZE-08 experiment (Martin et al., 2010b). The T0 sites were typically upwind of Manaus, with only occasional transport of pollution to these sites (Andreae et al., 2015; Chen et al., 2015). Auxiliary site "T2" served as a reference for polluted conditions. This site was located just across the Rio Negro (3.1392°S, 60.1315°W), 8 km from the southwestern edge of Manaus and typically downwind of urban emissions during the daytime.

### 2.2 Aerosol Mass Spectrometry

Characterization of the atmospheric PM was obtained using a High-Resolution Time-of-Flight Aerosol Mass Spectrometer (hereafter AMS; Aerodyne, Inc., Billerica, Massachusetts,

93 USA; DeCarlo et al., 2006; Canagaratna et al., 2007). Detailed aspects of the AMS operation in
94 GoAmazon2014/5 were presented in de Sá et al. (2017). In brief, the instrument was housed
95 within a temperature-controlled research container, and the inlet to the instrument sampled from
96 5 m above ground level. Ambient measurements for this study were obtained every other 4 min.
97 The other 4 min were used for analysis of output from an oxidation flow reactor as presented in
98 Palm et al. (2018).

99 Data analysis was performed using *SQUIRREL* (1.56D) and *PIKA* (1.14G) of the AMS
100 software suite (Sueper and collaborators; DeCarlo et al., 2006). Organic, sulfate, ammonium,
101 nitrate, and chloride PM mass concentrations were quantified. "Sulfate" and "nitrate"
102 concentrations reported by the AMS may include contributions from both organic and inorganic
103 species (Farmer et al., 2010; Liao et al., 2015). Organic and inorganic nitrate concentrations were
104 estimated based on the ratio of $NO_2^+$ to $NO^+$ signal intensity, as described in Section S2 (Fry et
105 al., 2009; Farmer et al., 2010; Fry et al., 2013). The organic elemental ratios, O:C and H:C, were
106 calculated following the methods of Canagaratna et al. (2015).

107 **2.3 Auxiliary measurements and datasets**

108 In complement to the AMS data set, the analysis herein incorporated auxiliary gas and
109 particle measurements collected during IOP1 at T3 (Martin et al., 2016). Mass concentrations of
110 molecular and tracer organic species in the gas and particle phases were measured by a Semi-
111 Volatile Thermal Desorption Aerosol Gas Chromatograph (SV-TAG) at a time resolution of one
112 hour (Isaacman-VanWertz et al., 2016). Concentrations of volatile organic compounds (VOCs)
113 were measured by a Proton-Transfer-Reaction Time-of-Flight Mass Spectrometer (PTR-ToF-
114 MS; Liu et al., 2016b). In the Mobile Aerosol Observing System (MAOS) of the ARM Climate
115 Research Facility (ACRF; Martin et al., 2016), measurements of $NO_y$ were made using a

chemiluminescence-based instrument (Air Quality Design). The raw $NO_y$ measurements (10-s resolution) were averaged across 30-min intervals to dampen the influence of brief local events. In addition, ozone concentrations were measured by an ultraviolet photometric analyzer (Thermo Fisher, model 49i, Ozone Analyzer). Particle number concentrations were measured by a Condensation Particle Counter (TSI, model 3772). Black carbon (BC) concentrations were measured both by a 7-wavelength aethalometer (Magee Scientific, model AE-31) and a Single Particle Soot Photometer (SP2; Droplet Measurement Techniques). The two datasets differed by a factor of up to three in absolute mass concentrations, as observed in other studies (Subramanian et al., 2007; Cappa et al., 2008; Lack et al., 2008), but they agreed well in the temporal trend. The analysis herein for BC is thus restricted to the temporal trends. Wind direction, solar irradiance, and precipitation rate were measured by the ARM Mobile Facility (AMF-1), which was also part of the ACRF.

Additional measurements from T0a, T0t, and T2 were also used in the analysis. At T2, non-refractory particle composition and concentration were measured by an Aerosol Chemical Speciation Monitor (ACSM) during the wet season from March 9 to April 30, 2014 (Cirino et al., submitted). ACSM measurements were made at T0a during the wet season of 2015, from February 1 to March 31 (Andreae et al., 2015). Further AMS datasets collected at T0t during the wet season of 2008 (February 6 to March 22; AMAZE-08 campaign) were used in the analysis (Chen et al., 2009;Schneider et al., 2011).

**2.4 Air mass backtrajectories and precipitation rates**

Simulations of two-day backward air mass trajectories, starting at 100 m above T3, were made using HYSPLIT4 (Draxler and Hess, 1998). Input meteorological data were obtained from the Global Data Assimilation System (GDAS), provided by the NOAA Air Resources

139 Laboratory (ARL), on a regular grid of 0.5° × 0.5°, 18 pressure levels, and 3-h intervals.
140 Trajectory steps were calculated for every 12 min.

141 Information on precipitation along the trajectories was obtained from the S-band radar of
142 the System for Amazon Protection (SIPAM) in Manaus (Machado et al., 2014). The radar had a
143 beam width of 1.8°, and it scanned 17 elevation angles every 12 min. Data were recorded to a
144 range of 240 km at 500-m gate spacing. The reflectivity fields were quality controlled to remove
145 non-meteorological echo and calibrated against the satellite precipitation radar of the Tropical
146 Rainfall Measuring Mission and Global Precipitation Measurement (TRMM-GPM; Kummerow
147 et al., 1998; Hou et al., 2014). Ground clutter was used to analyze the stability of the calibration.
148 The data were gridded at 2 km × 2 km in the horizontal and 0.5 km in the vertical using the
149 NCAR *Radx* software. The reflectivity at 2.5 km in altitude was converted to rain rates based on
150 the data sets of a Joss-Waldvogel disdrometer (Joss and Waldvogel, 1967), located at T3, 70 km
151 downwind of the radar.

152 **3. Results and discussion**

153 **3.1 Fine-mode PM composition**

154 The time series of mass concentrations of $PM_1$ species at T3 during the wet season of
155 2014 are plotted in Figure 1a. Organic material dominated the composition, contributing 79 ± 7%
156 (average ± one standard deviation), followed by sulfate (13 ± 5%). The standard deviation
157 quantifies the variability across the time series. Average non-refractory (NR) $PM_1$ mass
158 concentrations and compositions at T3 as well as at three other sites in the region are represented
159 in Figure 1b. The two T0 sites corresponded to predominantly background conditions. By
160 contrast, the T2 site represented conditions just downwind of Manaus, and depending on wind
161 direction experienced fresh Manaus pollution or background air. The comparison in Figure 1b

demonstrates that the organic component consistently constituted 70% to 80% of NR-$PM_1$ across sites in this region in the wet season, for both background and polluted conditions, in line with previous observations (Chen et al., 2009; Martin et al., 2010a).

Even as the relative composition was similar across all sites, there were differences in the absolute mass concentrations (Figure 1b, top panel). The NR-$PM_1$ mass concentrations at the T0 sites upwind of Manaus, although measured in different years, were consistently around 1 μg $m^{-3}$. The concentrations at the T2 site just downwind of Manaus were more than three times higher on average (3.3 μg $m^{-3}$). Average concentrations at the T3 site (1.7 μg $m^{-3}$), several hours downwind of Manaus, were lower compared to those at T2. This relative progression from T0, to T2, and then to T3 can be understood as a first-order quantification of the overall effect of Manaus emissions in increasing the airborne PM burden in the downwind region.

The diel trends of organic and sulfate mass concentrations as well as their variabilities across the four sites are shown in Figure 2. Lines represent means, solid markers show medians, and boxes span interquartile ranges. Organic mass concentrations and associated variability were higher at the T3 site compared to the T0 sites, markedly so in the afternoon hours. The greater variability at T3 is in line with a time-varying influence of Manaus emissions. This influence waxes and wanes with small northerly or southerly shifts of the trade winds as well as other changes in regional circulation tied to daily meteorology (dos Santos et al., 2014; Martin et al., 2017). The higher afternoon mass concentrations at T3 can be attributed to a combination of (i) an oxidant-rich, sunlight-fed plume that increases the production rate of secondary PM and (ii) faster near-surface winds during the day that transport PM from Manaus to T3 with less loss by deposition and dispersion compared to more-stagnant air at night. Among all sites, the T2 observations had both the highest average organic mass concentrations and the largest

variability. These characteristics of the T2 dataset can be explained by a combination of (i) the proximity of the site to Manaus, (ii) the rapid and 180° changes in wind direction caused by the intersection of the trade winds with a local river breeze (dos Santos et al., 2014), and (iii) possible contributions of emissions from brick kilns, located mostly southwest of the site, especially during night time (Martin et al., 2016; Cirino et al., submitted).

The diel trends of the sulfate mass concentrations were in large part similar to those of the organic mass concentrations. One distinction in the case of sulfate, however, is that the variability at the T0 sites is similar to that at the T3 site. The explanation is that the background sources of sulfate, including not only in-basin emissions but also out-of-basin long-range transport, are variable and significant enough to make the variability at the background sites similar to that at the T3 site (de Sá et al., 2017).

Overall, the organic $PM_1$ at T3 was highly oxidized, as indicated by the position of gray markers in the plot of Figure 3. By contrast, the blue markers represent the dataset collected at T2 during the same period. The datasets encompass all times of days and all conditions at both sites. Datasets from background sites collected in different years are shown in Figure S2. Points to the upper left represent more oxidized material, and points to the lower right represent less oxidized material (Ng et al., 2011a). The comparison depicted in Figure 3 indicates the effects of the plume over the 4 h of transport from T2 to T3, which were investigated in detail by Cirino et al. (submitted). The plot suggests that the enhanced oxidative cycle associated with higher OH and $O_3$ concentrations in the pollution plume might cause (i) the production of highly oxidized SOM, from both biogenic and anthropogenic precursors including aromatic compounds (Chhabra et al., 2011; Lambe et al., 2011), and (ii) the accelerated oxidative processing of pre-existing organic PM by OH and $O_3$ (Martin et al., 2017). The implication is that the emissions

208 from Manaus can significantly affect the mechanisms that produce or modify fine-mode PM over
209 the tropical forest.

210 **3.2 Characterization of organic PM by positive-matrix factorization**

211 Positive-matrix factorization was applied to the time series of the organic component of
212 the high-resolution mass spectra (Ulbrich et al., 2009c). Diagnostics of the PMF analysis are
213 presented in the Supplement (Section S1; Figures S3 and S4). Herein, "factor profile" and "factor
214 loading" refer to the mathematical products of the multivariate statistical analysis, whereas
215 "mass spectrum" and "mass concentration" refer to direct measurements.

216 A six-factor solution was obtained based both on the numerical diagnostics of the PMF
217 algorithm and the judged scientific meaningfulness of the resolved factors (Section S1). The
218 factor profiles, diel trends of the factor loadings, and the time series of the factor loadings and
219 other related measurements are plotted in Figures 4a, 4b, and 4c, respectively. The inset of
220 Figure 4a shows the mean fractional loading contribution of each factor during the analysis
221 period. The correlations of factor loadings with co-located measurements of gas- and particle-
222 phase species are shown in Figure 5.

223 The scientific interpretation of each factor was based on a combination of (i) the
224 characteristics of the factor profile (i.e., "mass spectrum"), as referenced to a worldwide database
225 of AMS spectra and PMF analyses (), and (ii) the temporal correlations between the factor
226 loading and other co-located measurements. Three factors interpreted as primary emissions of
227 organic PM were resolved: an anthropogenic-dominated factor (hereafter, "ADOA"), a biomass
228 burning factor ("BBOA"), and a fossil-fuel hydrocarbon-like factor ("HOA"). Three factors
229 interpreted as secondary production and processing were resolved: a more-oxidized oxygenated

230 factor ("MO-OOA"), a less-oxidized oxygenated factor ("LO-OOA"), and an isoprene
231 epoxydiols-derived factor ("IEPOX-SOA").

232 The HOA factor profile had characteristic ions of $C_4H_7^+$ and $C_4H_9^+$ at nominal values of
233 *m*/*z* 55 and 57, respectively (Figure 4a). It had an oxygen-to-carbon (O:C) ratio of 0.18 ± 0.02,
234 the lowest among the six factors (Table 1). In line with the AMS PMF literature, the HOA factor
235 represents a class of primary hydrocarbon-like organic compounds that are typically associated
236 with traffic emissions (Zhang et al., 2005). In the present study, the HOA factor loadings
237 accounted for 6% of the organic mass concentrations on average (Figure 4a, inset). As a point of
238 comparison, the average in the southeastern USA typically varies from 9% to 15% (Xu et al.,
239 2015b). The lower relative contribution of 6% in this study might in part be due to a larger
240 relative role of secondary production in the environment of a tropical forest. In addition, the
241 distance from Manaus to the T3 site might allow time for substantial vertical mixing, dilution,
242 and subsequent evaporation of primary emissions into entrained background air (Robinson et al.,
243 2007; Liu et al., accepted; Shilling et al., in preparation). Finally, the possible differences in
244 emission profiles associated with different types of regional economic development between the
245 Brazilian Amazon and the southeastern USA (e.g., fleet density, fuel matrix, industry, and so
246 forth) should also be considered. The HOA factor loading decreased during the day, which can
247 be explained by the growth of the planetary boundary layer (PBL) and the subsequent dilution of
248 the concentrations of primary emissions (Figure 4b). The time series of HOA factor loading did
249 not correlate well ($R < 0.5$) with any of the co-located measurements at T3 (Figure 5). It is
250 plotted alongside the time series of $NO_y$ concentration in Figure 4c.

251 The BBOA factor profile was characterized by distinct peaks of $C_2H_4O_2^+$ (*m*/*z* 60) and
252 $C_3H_5O_2^+$ (*m*/*z* 73), as shown in Figure 4a. These peaks can be attributed to levoglucosan and

253 other anhydrous sugars that result from biomass pyrolysis (Schneider et al., 2006; Cubison et al.,
254 2011). Correlations of the factor loadings with the mass concentrations of levoglucosan and
255 vanillin ($R > 0.8$) measured by SV-TAG corroborate the association with biomass burning
256 (Figure 4c). The BBOA factor of this study had an O:C ratio of 0.61 ± 0.08 (Table 1), which is
257 consistent with large contributions from levoglucosan (O:C of 0.83) and similar sugars. The
258 factor loading on average accounted for 9% of the organic $PM_1$ mass concentration (Figure 4a,
259 inset). This result is consistent with the low incidence of fires in the Amazon during the wet
260 season (Martin et al., 2016). The BBOA factor loading typically decreased during the day
261 (Figure 4b), which is suggestive of the dilution of local sources during the development of the
262 PBL rather than long-range transport. Emissions from local fires around T3, including trash and
263 tree burning, as well as from wood-fueled brick kilns along the road from Manaus to T3 might
264 have contributed to this factor.

265 The ADOA factor profile, distinguished prominently by the $C_7H_7^+$ ion at *m*/*z* 91, also had
266 characteristic ions of $C_4H_7^+$ at *m*/*z* 55 and $C_3H_5^+$ at *m*/*z* 41 (Figure 4a). A peak at *m*/*z* 91 can arise
267 from many sources, including biogenic and anthropogenic emissions (Ng et al., 2011b). In itself,
268 *m*/*z* 91 therefore does not serve as a tracer for a specific source or process without consideration
269 of the atmospheric context. Factors having a characteristic *m*/*z* 91 peak (usually labeled "91fac")
270 typically have been associated with biogenic emissions (Robinson et al., 2011; Budisulistiorini et
271 al., 2015; Chen et al., 2015; Riva et al., 2016). The ADOA factor profile of this study, however,
272 more strongly resembles the mass spectra previously reported for PM emissions from cooking
273 activities (Lanz et al., 2007; Mohr et al., 2012) than those from "91fac" (Section S1; Figure S5).
274 The ratio of *m*/*z* 55 to *m*/*z* 57 of the ADOA factor was 4.1. This ratio lies in the range of 2 to 10
275 reported for several factors representing primary cooking emissions and is well above the range

of 0.8 to 1.4 reported for factors associated with traffic emissions, i.e., HOA (Mohr et al., 2012 and references therein; Hu et al., 2016). Even though the ADOA factor profile has a large contribution from non-oxygenated ions, similar to the HOA factor and consistent with a dominance by primary emissions, it also contains considerable signal from oxygenated ions, resulting in a relatively higher O:C of 0.40 ± 0.05 (Table 1). The factor loading on average accounted for 13% of the organic $PM_1$ mass concentration (Figure 4a, inset). The factor loading decreased as the PBL developed during the day, consistent with dominant non-photochemical, primary sources (Figure 4b). Furthermore, there were increases, albeit small, in factor loading at 12:00 and 18:00 (local time), suggestive of breakfast-time and lunch-time cooking activities in Manaus based on a transport time of 4 to 6 h between the city and the T3 site (Martin et al., 2016; Cirino et al., submitted). Manaus typically has four rush-hour periods each day from 6:30 to 8:00, 12:00 to 13:30, 16:30 to 18:30, and 21:00 to 22:00. Traffic peaking at these hours may therefore also have contributed to the ADOA factor. Correlations between factor loading and external measurements exceeded $R = 0.5$ for many anthropogenic markers, including concentrations of aromatics (e.g., benzene, toluene, and $C_8$ and $C_9$ species), carbon monoxide, particle count, and $NO_y$ (Figure 4c, Figure 5). Contributions from secondary processes cannot be ruled out, and it is possible that PM production from anthropogenic VOCs might have also been captured in this factor. Overall, the ADOA factor was interpreted in the present study as an indicator of anthropogenic influence associated with several sources in Manaus, most importantly cooking and possibly traffic emissions.

The IEPOX-SOA factor profile had marker ions of $C_4H_5^+$ ($m/z$ 53) and $C_5H_6O^+$ ($m/z$ 82) (Figure 4a; Lin et al., 2012; Hu et al., 2015; de Sá et al., 2017). It had an O:C ratio of 0.9 ± 0.10 (Table 1). The factor loading on average accounted for 17% of the organic $PM_1$ mass

299 concentration (Figure 4a, inset). There were high correlations ($R > 0.8$) between factor loadings
300 and concentrations of $C_5$-alkenetriols and 2-methyltetrols, which are markers of IEPOX-derived
301 PM, produced by the photo-oxidation of isoprene under $HO_2$-dominant conditions (Surratt et al.,
302 2010; Lin et al., 2012; Figure 4c). The increase in factor loading during daytime was consistent
303 with a photochemical source (Figure 4b). There were also correlations between factor loadings
304 and concentrations of sulfate and some acids, such as tricarballylic acid (TCA; Figure 5), in
305 agreement with the association of IEPOX-derived PM and sulfate/acidity observed in other
306 studies (Budisulistiorini et al., 2013; Nguyen et al., 2014; Kuwata et al., 2015). Overall, this
307 factor was therefore interpreted as representative of PM produced from isoprene photo-oxidation
308 under $HO_2$-dominant conditions. The effects of urban pollution on the loadings of this factor
309 were the focus of a previous publication (de Sá et al., 2017).
310 The two remaining factors, LO-OOA and MO-OOA, were also associated with secondary
311 atmospheric processes. The LO-OOA and MO-OOA factors had O:C ratios of $0.72 \pm 0.10$ and
312 $1.09 \pm 0.17$, respectively. The LO-OOA factor was characterized by the greatest ratio of signal
313 intensity of the $C_2H_3O^+$ ion ($m/z$ 43) to that of the $CO_2^+$ ion ($m/z$ 44) (Figure 4a) compared to all
314 other factors. This factor is usually attributed to lower-generation, less-oxidized, higher-volatility
315 secondary organic PM (Jimenez et al., 2009). By comparison, the MO-OOA factor profile had
316 the strongest $CO_2^+$ ($m/z$ 44) peak among all factors (Figure 4a). This factor is usually attributed
317 to higher-generation, more-oxidized, less-volatile secondary organic PM or extensively oxidized
318 primary PM of any type that has resided in the atmosphere for several days or more (Jimenez et
319 al., 2009).
320 The LO-OOA factor loading on average accounted for 25% of the organic $PM_1$ mass
321 concentration (Figure 4a, inset). The factor loading correlated better with the estimated

concentrations of inorganic nitrate than with organic or total nitrate (Figure 5; Section S2 and Figure S6), which is consistent with the interpretation of the higher volatility associated with this factor (Jimenez et al., 2009; Zhang et al., 2011). The factor loading also correlated ($R > 0.7$) with the concentrations of 2-methylglyceric acid and methyl-butyl-tricarboxylic acid (MBTCA), which are products of isoprene and monoterpene oxidation, respectively, under NO-dominant conditions (Figure 4c; Figure 5). The factor loading increased starting at 9:00 (local time) and peaked in the afternoon hours (Figure 4b). This diel trend, tied to the sunlight cycle, tracked the typical daily emission patterns of isoprene and monoterpenes from the surrounding forest (Yáñez-Serrano et al., 2015). The absence of a sharp decline at sunset and the higher variability at nighttime may also indicate a contribution by terpene ozonolysis. For these several reasons, the LO-OOA factor was interpreted herein as secondary organic PM produced mostly within several hours of observations by many possible pathways, including (i) the photo-oxidation of isoprene along non-IEPOX pathways, (ii) the photo-oxidation of terpenes and other biogenic VOCs along both $HO_2$- and NO-dominant reaction pathways, (iii) the ozonolysis of terpenes, and (iv) the possible production of SOM from anthropogenic emissions from Manaus.

The MO-OOA factor loading on average accounted for 30% of the organic $PM_1$ mass concentration (Figure 4a, inset). The factor loading correlated ($R > 0.7$) with the mass concentrations of several particle-phase carboxylic acids as well as the concentrations of sulfate, ammonium, and ozone (Figure 5). The time series of malic acid and ozone concentrations are shown alongside the MO-OOA factor loadings in Figure 4c. Malic acid is a highly oxidized compound (O:C of 1.25), which may have many different sources (Röhrl and Lammel, 2002; van Pinxteren et al., 2014). The MO-OOA factor loading increased starting at 8:00 (local time; sunrise was at 6:00) and peaked between 10:00 and 16:00, with a large variability in the factor

loadings in the afternoon hours among different days (Figure 4b). The afternoon increase and day-to-day variability were consistent with strong but variable photochemical processing leading to further oxidation of organic PM during the day, depending on daily weather. The high O:C of $1.09 \pm 0.17$ could also be indicative of production of PM from aromatic compounds emitted from Manaus (Chhabra et al., 2011; Lambe et al., 2011). Overall, this factor was interpreted to represent highly oxidized PM from multiple processes. Species initially associated with HOA, BBOA, ADOA, IEPOX-SOA, and LO-OOA factors may converge after sufficient atmospheric oxidation to become represented by the MO-OOA factor (Jimenez et al., 2009; Palm et al., 2018).

## 3.3 Shifts in PM with anthropogenic influences

### 3.3.1 Cluster Analysis

To further investigate changes in the concentration and composition of PM associated with anthropogenic influences, a Fuzzy c-means (FCM) algorithm was applied to the time series of concentrations of particle number, $NO_y$, ozone, black carbon, and sulfate measurements at the T3 site (Bezdek et al., 1984). The analysis was fully independent of the PMF results. For each point in time, these concentrations represented the spatial coordinates of the data point. As discussed below, four clusters were identified. Based on measures of spatial similarity, the clustering algorithm attributed to each data point a degree of membership relative to each of the four clusters (Section S3; Figure S7 and Figure S8).

The scope of the clustering analysis was restricted to afternoon time points for which ten-hour airmass backtrajectories did not intersect significant precipitation and for which solar irradiance at T3 averaged over the previous 4 h was higher than 200 W $m^{-2}$ (Section S3). This scope aimed at capturing fair-weather conditions and thereby minimizing the role of otherwise

368 confounding processes, such as boundary layer dynamics and wet deposition. The elimination of
369 trajectories having precipitation, however, should not be regarded as fully accurate given the
370 uncertainties in the HYSPLIT trajectories. The scoped dataset spanned 24 afternoons.
371 Four clusters were identified based on minimization of the FCM objective function as
372 well as a subjective assessment of meaningful interpretation of the set of clusters (Section S3).
373 The FCM algorithm returned a matrix containing the degrees of membership (ranging from 0 to
374 1) to each of the four clusters (columns) for each point in time (rows). For any given time point
375 (i.e., row), the sum of its degrees of membership to clusters (i.e., sum across columns) was
376 always unity, by definition. A collection of examples, representing 37% of the analyzed data
377 points by FCM, is shown in Figure 6a. For times predominantly associated with only one cluster
378 (e.g., Feb 9 and Feb 10), the corresponding air mass backtrajectories are plotted in Figure 7. The
379 FCM algorithm also returned the coordinates of cluster centroids, which are listed in Table 2.
380 Two clusters of data were interpreted as "background" and labeled "Bkgd-1" and "Bkgd-
381 2". They were characterized by $NO_y$ < 1 ppb, ozone < 20 ppb, and particle number < 1200 $cm^{-3}$
382 (Table 2; Figure 6). The two clusters differed especially in that Bkgd-2 had significantly larger
383 concentrations of sulfate and black carbon. A comparison of the datasets of Feb 13
384 (predominantly Bkgd-1) and Feb 16 (predominantly Bkgd-2) in Figure 6 highlights these
385 differences. Concentrations of sulfate and black carbon were 0.15 and 0.10 μg $m^{-3}$, respectively,
386 on Feb 13, compared to 0.40 and 0.15 μg $m^{-3}$ on Feb 16. The backtrajectories associated with
387 Bkgd-1 had both northeasterly and southeasterly components. The wind fields, out of line with
388 the trade winds, may suggest passage through recent weather systems and may imply wet
389 deposition, which in turn might explain lower gas and particle concentrations (Table 2). These
390 recent weather systems might not have been excluded from the scoped dataset because of

391 inaccuracies in the intersections of the backtrajectories with precipitation data, as discussed
392 above, or because they were more distant than captured by the 10-h backtrajectories. Consistent
393 with this hypothesis, the centroid value calculated for the 4-h averaged solar irradiance at T3
394 (Section 3.3.2) was lower for Bkgd-1 (400 W $m^{-2}$) compared to the other clusters (600 W $m^{-2}$),
395 suggesting an association of Bkgd-1 with overcast conditions. By comparison, the
396 backtrajectories associated with Bkgd-2 were predominantly from the northeast, coming from the
397 direction of the T0t and T0a sites (Figure 7), in line with the dominant trade winds of the wet
398 season. The air masses of Bkgd-2 may have experienced less wet deposition and may represent
399 more extensive atmospheric oxidation than those of Bkgd-1. They may also have carried PM
400 contributions from out-of-basin sources, which would be consistent with the higher sulfate and
401 black carbon concentrations of Bkgd-2 compared to Bkgd-1 (Chen et al., 2009; Pöhlker et al.,
402 2017).
403 Two other clusters were interpreted as "polluted" and labeled "Pol-1" and "Pol-2". They
404 were characterized by concentrations of $NO_y$ > 1 ppb, ozone > 20 ppb, and particle number >
405 1200 $cm^{-3}$ (Table 2; Figure 6). The dataset of the afternoon of Mar 9 illustrates a shift in
406 dominance from Pol-2 to Pol-1 (Figure 6). Although Pol-1 and Pol-2 both have high
407 concentrations of sulfate and other pollutants, they differ in the extent of those high
408 concentrations. The explanation may be that these clusters represent different source regions.
409 Pol-1 may be associated with emissions from the northern region of Manaus, and Pol-2 may be
410 associated with emissions from the southern region of Manaus. Industry, power production, and
411 oil refineries are concentrated in the southeastern region of Manaus (Figure S9; Medeiros et al.,
412 2017). Population density and commercial activity is concentrated in the southwestern portion of
413 the city where downtown is located (Figure S10). Aircraft observations show that concentrations

414 of sulfate as well as other pollutants are higher in the urban outflow from the southern compared
415 to the northern region of Manaus (Figure S10). Directional plots of $SO_2$ and particle number
416 concentrations observed at the T2 site further demonstrate the heterogeneity in Manaus
417 emissions (Figure S10). This hypothesis of a geographical difference in source regions
418 qualitatively aligns with the differences in backtrajectories characteristic of times dominated by
419 Pol-1 and Pol-2 (Figure 7). This interpretation does imply, however, that the backtrajectories
420 may have a 20° inaccuracy. Such inaccuracy is reasonable for the application of HYSPLIT
421 modeling in this region given (i) the absence of surface weather stations and (ii) the relatively
422 large scale of input wind fields (i.e., 50 km) compared to the scale of modeling (i.e., 70 km from
423 T3 to Manaus and a city cross section of 20 km).

424 **3.3.2 Comparison of PM among clusters**

425 The characteristic PM composition associated with each cluster was determined by
426 calculating the centroid coordinates of the clusters for the AMS species and PMF factors
427 (Section S3). The centroid coordinate of a cluster for a given variable is defined as a weighted
428 mean of that variable across all points in time, where the weight is the degree of membership of
429 each data point to that cluster. A comparison of $PM_1$ concentrations and compositions for the
430 four clusters is shown in Figure 8. Values are listed in Table 2.

431 The NR-$PM_1$ mass concentrations increased by 25% to 200% in clusters Pol-1 and Pol-2
432 compared to clusters Bkgd-1 and Bkgd-2 (Figure 8a). Increases in sulfate and associated
433 ammonium concentrations had a smaller yet non-negligible role in the increased $PM_1$ mass
434 concentrations. Sources of sulfate other than Manaus sustain relatively high concentrations in the
435 Amazon basin, as represented by the Bkgd-2 cluster (Chen et al., 2009; de Sá et al., 2017).
436 Compared to these regional background concentrations (i.e., Bkgd-2 cluster), the increases in

sulfate concentrations were significant only for air masses associated with the heavily industrialized and densely populated southern region of Manaus (i.e., Pol-2 cluster).

With respect to the composition of the organic PM, Figure 8b shows that the Bkgd-1 cluster had large contribution from the LO-OOA factor. By comparison, the Bkgd-2 cluster had larger contributions from the MO-OOA and IEPOX-SOA factors. A comparison of 13 Feb and 16 Feb of 2014 (Figure 6d) illustrates these findings. The low mass concentrations and the dominant contribution by the LO-OOA factor suggest that the Bkgd-1 cluster may represent conditions under which secondary organic PM was produced within recent hours through photo-oxidation of VOCs emitted by the forest and subsequent condensation of secondary organic material. The low sulfate concentrations for Bkgd-1 may rationalize the absence of a significant contribution by the IEPOX-SOA factor. Isoprene photo-oxidation may have contributed to PM production by pathways other than IEPOX uptake (Krechmer et al., 2015; Riva et al., 2016). By comparison, for Bkgd-2, the higher mass concentrations and the greater contributions by IEPOX-SOA and MO-OOA factors suggest that this cluster may represent conditions under which secondary organic PM was a combination of material produced both on that day as well as on previous days. During transport, the organic PM may have undergone extensive atmospheric oxidation by a combination of surface and condensed-phase chemistry, including cloud water processes (Carlton et al., 2006; Ervens et al., 2011; Hoyle et al., 2011; Perraud et al., 2012). Concentrations and composition of the Bkgd-2 cluster may therefore represent an extensive geographical footprint.

The organic PM concentration and composition associated with the Pol-1 and Pol-2 clusters were distinct from those of the Bkgd-1 and Bkgd-2 clusters (Figure 8). The mass concentrations of organic PM were greater by 25% to 150% for Pol-1 and Pol-2. According to

460 the PMF factors (Figure 8b), the larger part of this increase in organic PM between the
461 background and polluted clusters was tied to the production of secondary organic PM, although
462 primary emissions also contributed significantly. By comparison, for both Bkgd-1 and Bkgd-2
463 clusters, contributions by primary emissions were negligible, as indicated by the low summed
464 contribution of factors of primary origin (i.e., ADOA, BBOA, and HOA) to the organic $PM_1$ (<
465 10%). For Pol-1 and Pol-2, the ADOA factor loading on average accounted for 10% of the
466 organic mass concentration at T3, serving as a strong marker of Manaus pollution. A comparison
467 of February 9 and March 9 with February 13 and 16 illustrates these findings (Figure 6d).
468 In regard to secondary organic PM, the IEPOX-SOA factor loading decreased by almost
469 50% under polluted compared to background conditions. de Sá et al. (2017) attributed this
470 decrease to the suppression of IEPOX production by elevated NO concentrations. This
471 suppression typically outweighed possible enhancements in IEPOX uptake and subsequent PM
472 production because of elevated sulfate concentrations. By contrast, the LO-OOA and MO-OOA
473 factor loadings increased by 50% to 100% under polluted conditions. These increases exceeded
474 the decrease in IEPOX-SOA factor loadings, resulting in a net increase of around 100% in mass
475 concentration of secondary organic PM (Figure 8).
476 The shifts in the processes governing the production of secondary organic PM because of
477 increased $NO_x$, OH, and $O_3$ concentrations characteristic of the pollution plume were complex
478 and non-linear (Figure 9a). Overall, the oxidation pathways were driven faster. The relatively
479 high $f_{CO_2^+}$ values and O:C ratios of all factors (Table 1), including those associated with primary
480 emissions, compared to typical values at other locations worldwide (Canagaratna et al., 2015),
481 corroborate this interpretation. Ozone concentrations in the plume increase by 200% to 300%,
482 and hydroxyl radical concentrations increased by 250% or more (Liu et al., accepted). As $HO_2$-

483 dominant pathways were inhibited, NO-dominant pathways became active. Increased oxidant
484 concentrations may also have promoted additional multigenerational chemistry of semi- or
485 intermediate-volatility species (Robinson et al., 2007). Oxidation of VOCs by aqueous-phase
486 reactions, including in-cloud processing, and oxidation of biomass burning emissions may also
487 have played roles to varying degrees on different days (Carlton et al., 2006; Ervens et al., 2011;
488 Hoyle et al., 2011; Perraud et al., 2012). In addition, when primary and secondary PM mass
489 concentrations increased, further uptake of oxidized semi-volatile molecules could have been
490 thermodynamically favored according to partitioning theory, representing a positive feedback on
491 the increase of mass concentrations (Pankow, 1994; Odum et al., 1996; Carlton et al., 2010).
492 The increase in the LO-OOA and MO-OOA factor loadings associated with Pol-1 and
493 Pol-2 indicates that the net effect of this accelerated and modified chemistry was the quick
494 production and further oxidation of secondary organic PM. Precursors may have included both
495 the wide range of biogenic VOCs as well as contributions from anthropogenic precursors, such
496 as gas-phase species from vehicle emissions or evaporated primary material (Nordin et al., 2013;
497 Presto et al., 2014). The LO-OOA factor loading was important for the polluted conditions of
498 Pol-1 and Pol-2 as well as for the clean conditions of Bkgd-1. This result is not necessarily
499 because of an in-common molecular composition but rather because of an in-common process,
500 i.e., fresh production of secondary organic PM (Figure 9b). Likewise, the MO-OOA factor
501 loading was important for Pol-1, Pol-2, and Bkgd-2 because this factor represented an in-
502 common process, i.e., extensive oxidation (Figure 9b). In the case of the MO-OOA factor, there
503 is also an overall in-common composition characterized by highly oxidized species even as
504 precursor species and subsequent oxidation pathways differed (Jimenez et al., 2009).

505 The complexity of the real atmospheric processes, as illustrated in Figure 9, is to some
506 extent captured by the instrumental and analytical tools herein employed. Positive-matrix
507 factorization identified several broad classes of organic PM. Some PMF factors had sufficiently
508 unique signatures that they could be associated to one specific source and/or process (e.g., HOA
509 and IEPOX-SOA). Other factors, in contrast, represented a wide range of sources that shared in-
510 common processes (e.g., LO-OOA and MO-OOA). The clustering analysis contextualized the
511 PMF results and demonstrated that the effects of the urban pollution were neither limited to nor
512 captured by a single PMF factor. Instead, the urban plume influenced several PMF factors in
513 different ways and to different extents. The implication is that changes in the AMS spectral
514 signature of the organic PM caused by polluted conditions may not be sufficiently unique to
515 allow for its complete separation by PMF analysis alone, especially in respect to the production
516 of secondary organic PM. In this context, the Fuzzy c-means analysis served herein as a useful
517 tool to incorporate auxiliary datasets and thereby to further understand anthropogenic influences
518 on PM production and characteristics.

519 **4. Summary and conclusions**

520 Changes in the concentrations and the composition of fine-mode PM due to the influence
521 of anthropogenic emissions were investigated for the Amazonian wet season. Organic material
522 dominated the submicron composition, consistently representing between 70% and 80% of the
523 $PM_1$ mean mass concentration across measurement sites upwind and downwind of Manaus and
524 across different levels of pollution. Absolute mass concentrations, however, varied significantly
525 among sites. Average concentrations downwind of Manaus were 100% to 200% higher than
526 those upwind. Furthest downwind at T3, the organic component was more oxidized compared to
527 that at the T2 site.

Positive-matrix factorization and Fuzzy c-means clustering were applied to the datasets to obtain a composite analysis of the shifts in $PM_1$ concentrations and composition under polluted conditions. Based on the FCM clustering, every point in time at T3 was interpreted as being affected by a combination of four influences, as represented by four clusters. Two background (Bkgd-1 and Bkgd-2) and two polluted (Pol-1 and Pol-2) clusters were identified. Particle mass concentrations were double for polluted compared to background conditions. Contributions from secondary processes dominated (> 80%) for both background and polluted conditions.

In terms of primary emissions, absolute contributions increased by a factor of five or more under polluted conditions, corresponding to an increase from < 10% to 15% of total $PM_1$. The ADOA factor loading increased over five-fold for the polluted compared to the background clusters, and this factor thus served as a strong tracer of Manaus pollution. BBOA and HOA factor loadings, associated with biomass burning and fossil fuels, respectively, increased by two-fold with pollution. The ADOA factor loading represented 61% to 76% of the total primary factor loadings for the Pol-1 and Pol-2 clusters.

As for the secondary processes, the analysis further finds that the pollution plume acted both to shift pathways of secondary organic PM production and to accelerate the atmospheric oxidation of pre-existing organic PM. The oxidation of biogenic PM precursors shifted from $HO_2$- to NO-dominant pathways, and the oxidation of anthropogenic precursors possibly contributed to increased PM concentrations. The IEPOX-SOA factor loadings were highest for the Bkgd-2 cluster, associated with long-range transport under background conditions, and decreased by almost 50% for the polluted clusters, in line with a shift of isoprene oxidation from $HO_2$- to NO-dominant pathways. Concomitantly, the LO-OOA factor loading increased by more than 50% for these clusters, suggesting rapid in-plume production of secondary organic PM

551 through several pathways. The LO-OOA factor was also important for the Bkgd-1 cluster,
552 associated with fresh background conditions, which is suggestive of recent biogenic organic PM
553 production. The MO-OOA factor had large relative contributions in the Bkgd-2, Pol-1, and Pol-2
554 clusters, suggestive of significant oxidative processing associated with these clusters. Increases
555 of up to 300% in the MO-OOA factor loadings for Pol-1 and Pol-2 relative to background
556 conditions of Bkgd-1 showed the effects of an accelerated oxidation cycle, leading to highly
557 oxidized PM downwind of Manaus. Based on this and related studies (Liu et al., 2016b; de Sá et
558 al., 2017; Martin et al., 2017), the critical lever seems to be increased concentrations of nitrogen
559 oxides in the pollution plume for both directly shifting and indirectly accelerating mechanisms of
560 secondary organic PM production in central Amazonia during the wet season.
561 The altered composition under anthropogenic influences also affects the physical
562 properties of the $PM_1$. Bateman et al. (2017), using the results of the PMF analysis presented
563 herein, reported a shift from predominantly liquid PM under background conditions to a
564 considerable presence of non-liquid PM above 50% RH under polluted conditions. Non-liquid
565 PM can have different reactive chemistry from liquid PM (Li et al., 2015; Liu et al., 2018). A
566 linear relationship between the increase in particle rebound fraction and the sum of ADOA,
567 BBOA, and HOA factor loadings had an $R^2$ of 0.7. The highest individual correlation was with
568 the ADOA factor loading (Bateman, personal communication). In addition, Thalman et al.
569 (2017), also using the PMF results reported herein, concluded that the larger relative contribution
570 of secondary organic material during the daytime compared to the nighttime was the primary
571 driver of the diel trend of higher particle hygroscopicity during the day compared to the night, as
572 tied to cloud condensation nuclei (CCN) properties.

This study communicates a snapshot of the changes that occur in the atmospheric composition over a tropical forest because of regional urbanization. In the context of a forest in transition (Davidson et al., 2012), the findings herein provide a quantitative assessment of the effects of urban pollution on the forested surroundings of Manaus. The studied region and the observed changes in atmospheric composition represent a microcosm that might become more widespread through Amazonia as urbanization trends continue in the future. Further investigations of the specific chemical pathways and physical mechanisms that enhance PM production in the urban plume are warranted to understand what other pollutants are critical for control in the context of ongoing and future air quality regulation in the study region as well as for other tropical forested environments worldwide.

**Acknowledgments.** Institutional support was provided by the Central Office of the Large Scale Biosphere Atmosphere Experiment in Amazonia (LBA), the National Institute of Amazonian Research (INPA), and Amazonas State University (UEA). We acknowledge support from the Atmospheric Radiation Measurement (ARM) Climate Research Facility, a user facility of the United States Department of Energy (DOE, DE-SC0006680), Office of Science, sponsored by the Office of Biological and Environmental Research, and support from the Atmospheric System Research (ASR, DE-SC0011115, DE-SC0011105) program of that office. Additional funding was provided by the Amazonas State Research Foundation (FAPEAM 062.00568/2014 and 134/2016), the São Paulo State Research Foundation (FAPESP 2013/05014-0), the USA National Science Foundation (1106400 and 1332998), and the Brazilian Scientific Mobility Program (CsF/CAPES). S. S. de Sá acknowledges support by the Faculty for the Future Fellowship of the Schlumberger Foundation. BBP is grateful for a US EPA STAR Graduate Fellowship (FP-91761701-0). The authors thank Paulo Castillo for his assistance in quality-checking the black carbon data from MAOS. Data access from the Sistema de Proteção da Amazônia (SIPAM) is gratefully acknowledged. The research was conducted under scientific license 001030/2012-4 of the Brazilian National Council for Scientific and Technological Development (CNPq).

## References


Andreae, M. O., Acevedo, O. C., Araùjo, A., Artaxo, P., Barbosa, C. G. G., Barbosa, H. M. J., Brito, J., Carbone, S., Chi, X., Cintra, B. B. L., da Silva, N. F., Dias, N. L., Dias-Júnior, C. Q., Ditas, F., Ditz, R., Godoi, A. F. L., Godoi, R. H. M., Heimann, M., Hoffmann, T., Kesselmeier, J., Könemann, T., Krüger, M. L., Lavric, J. V., Manzi, A. O., Lopes, A. P., Martins, D. L., Mikhailov, E. F., Moran-Zuloaga, D., Nelson, B. W., Nölscher, A. C., Santos Nogueira, D., Piedade, M. T. F., Pöhlker, C., Pöschl, U., Quesada, C. A., Rizzo, L. V., Ro, C. U., Ruckteschler, N., Sá, L. D. A., de Oliveira Sá, M., Sales, C. B., dos Santos, R. M. N., Saturno, J., Schöngart, J., Sörgel, M., de Souza, C. M., de Souza, R. A. F., Su, H., Targhetta, N., Tóta, J., Trebs, I., Trumbore, S., van Eijck, A., Walter, D., Wang, Z., Weber, B., Williams, J., Winderlich, J., Wittmann, F., Wolff, S., and Yáñez-Serrano, A. M.: The Amazon Tall Tower Observatory (ATTO): overview of pilot measurements on ecosystem ecology, meteorology, trace gases, and aerosols, Atmos. Chem. Phys., 15, 10723-10776, 2015, 10.5194/acp-15-10723-2015.

Artaxo, P., Rizzo, L. V., Brito, J. F., Barbosa, H. M. J., Arana, A., Sena, E. T., Cirino, G. G., Bastos, W., Martin, S. T., and Andreae, M. O.: Atmospheric aerosols in Amazonia and land use change: from natural biogenic to biomass burning conditions, Faraday Disc., 165, 203-235, 2013, 10.1039/C3FD00052D.

Bateman, A. P., Gong, Z., Harder, T. H., de Sá, S. S., Wang, B., Castillo, P., China, S., Liu, Y., O'Brien, R. E., Palm, B. B., Shiu, H. W., Cirino, G. G., Thalman, R., Adachi, K., Alexander, M. L., Artaxo, P., Bertram, A. K., Buseck, P. R., Gilles, M. K., Jimenez, J. L., Laskin, A., Manzi, A. O., Sedlacek, A., Souza, R. A. F., Wang, J., Zaveri, R., and Martin, S. T.: Anthropogenic influences on the physical state of submicron particulate matter over a tropical forest, Atmos. Chem. Phys., 17, 1759-1773, 2017, 10.5194/acp-17-1759-2017.

Bezdek, J. C., Ehrlich, R., and Full, W.: FCM: The fuzzy c-means clustering algorithm, Computers & Geosciences, 10, 191-203, 1984.

Brito, J., Carbone, S., de Sá, S. S., Martin, S. T., and Artaxo, P., in preparation.

Budisulistiorini, S. H., Canagaratna, M. R., Croteau, P. L., Marth, W. J., Baumann, K., Edgerton, E. S., Shaw, S. L., Knipping, E. M., Worsnop, D. R., Jayne, J. T., Gold, A., and Surratt, J. D.: Real-time continuous characterization of secondary organic aerosol derived from isoprene epoxydiols in downtown Atlanta, Georgia, using the Aerodyne Aerosol Chemical Speciation Monitor, Environ. Sci. Technol., 47, 5686-5694, 2013, 10.1021/es400023n.

Budisulistiorini, S. H., Li, X., Bairai, S. T., Renfro, J., Liu, Y., Liu, Y. J., McKinney, K. A., Martin, S. T., McNeill, V. F., Pye, H. O. T., Nenes, A., Neff, M. E., Stone, E. A., Mueller, S., Knote, C., Shaw, S. L., Zhang, Z., Gold, A., and Surratt, J. D.: Examining the effects of anthropogenic emissions on isoprene-derived secondary organic aerosol formation during the 2013 Southern Oxidant and Aerosol Study (SOAS) at the Look Rock, Tennessee ground site, Atmos. Chem. Phys., 15, 8871-8888, 2015, 10.5194/acp-15-8871-2015.

Canagaratna, M. R., Jayne, J. T., Jimenez, J. L., Allan, J. D., Alfarra, M. R., Zhang, Q., Onasch, T. B., Drewnick, F., Coe, H., Middlebrook, A., Delia, A., Williams, L. R., Trimborn, A. M., Northway, M. J., DeCarlo, P. F., Kolb, C. E., Davidovits, P., and Worsnop, D. R.: Chemical and microphysical characterization of ambient aerosols with the aerodyne aerosol mass spectrometer, Mass Spectrom. Rev., 26, 185-222, 2007, 10.1002/mas.20115.

Canagaratna, M. R., Jimenez, J. L., Kroll, J. H., Chen, Q., Kessler, S. H., Massoli, P., Hildebrandt Ruiz, L., Fortner, E., Williams, L. R., Wilson, K. R., Surratt, J. D., Donahue, N. M., Jayne, J. T., and Worsnop, D. R.: Elemental ratio measurements of organic compounds using aerosol mass spectrometry: characterization, improved calibration, and implications, Atmos. Chem. Phys., 15, 253-272, 2015, 10.5194/acp-15-253-2015.

Cappa, C. D., Lack, D. A., Burkholder, J. B., and Ravishankara, A. R.: Bias in filter-based aerosol light absorption measurements due to organic aerosol loading: evidence from laboratory Measurements, Aerosol Sci Technol, 42, 1022-1032, 2008, 10.1080/02786820802389285.

Carbone, S., Brito, J., De Sá, S. S., Martin, S. T., and Artaxo, P., in preparation.

Carlton, A. G., Turpin, B. J., Lim, H.-J., Altieri, K. E., and Seitzinger, S.: Link between isoprene and secondary organic aerosol (SOA): Pyruvic acid oxidation yields low volatility organic acids in clouds, Geophys. Res. Lett., 33, L06822, 2006, 10.1029/2005GL025374.

Carlton, A. G., Pinder, R. W., Bhave, P. V., and Pouliot, G. A.: To What Extent Can Biogenic SOA be Controlled?, Environ. Sci. Technol., 44, 3376-3380, 2010, 10.1021/es903506b.

Chen, Q., Farmer, D. K., Schneider, J., Zorn, S. R., Heald, C. L., Karl, T. G., Guenther, A., Allan, J. D., Robinson, N., Coe, H., Kimmel, J. R., Pauliquevis, T., Borrmann, S., Pöschl, U., Andreae, M. O., Artaxo, P., Jimenez, J. L., and Martin, S. T.: Mass spectral characterization of submicron biogenic organic particles in the Amazon Basin, Geophys. Res. Lett., 36, L20806, 2009, 10.1029/2009GL039880.

Chen, Q., Farmer, D. K., Rizzo, L. V., Pauliquevis, T., Kuwata, M., Karl, T. G., Guenther, A., Allan, J. D., Coe, H., Andreae, M. O., Pöschl, U., Jimenez, J. L., Artaxo, P., and Martin, S. T.: Submicron particle mass concentrations and sources in the Amazonian wet season (AMAZE-08), Atmos. Chem. Phys., 15, 3687-3701, 2015, 10.5194/acp-15-3687-2015.

Chhabra, P., Ng, N., Canagaratna, M., Corrigan, A., Russell, L., Worsnop, D., Flagan, R., and Seinfeld, J.: Elemental composition and oxidation of chamber organic aerosol, Atmos. Chem. Phys., 11, 8827-8845, 2011.

Cirino, G. G., Brito, J., Barbosa, H. J. M., Rizzo, L. V., Tunved, P., de Sá, S. S., Jimenez, J., Palm, B. B., Carbone, S., Lavric, J., Souza, R., Wolff, S., Walter, D., Tota, J., Oliveira, M., Martin, S. T., and Artaxo, P.: Observations of Manaus urban plume evolution and interaction with biogenic emissions in GoAmazon2014/5, Atmos Environ, submitted.

Cubison, M. J., Ortega, A. M., Hayes, P. L., Farmer, D. K., Day, D., Lechner, M. J., Brune, W. H., Apel, E., Diskin, G. S., Fisher, J. A., Fuelberg, H. E., Hecobian, A., Knapp, D. J., Mikoviny, T., Riemer, D., Sachse, G. W., Sessions, W., Weber, R. J., Weinheimer, A. J., Wisthaler, A., and Jimenez, J. L.: Effects of aging on organic aerosol from open biomass burning smoke in aircraft and laboratory studies, Atmos. Chem. Phys., 11, 12049-12064, 2011, 10.5194/acp-11-12049-2011.

Davidson, E. A., de Araújo, A. C., Artaxo, P., Balch, J. K., Brown, I. F., Bustamante, M. M., Coe, M. T., DeFries, R. S., Keller, M., and Longo, M.: The Amazon basin in transition, Nature, 481, 321-328, 2012.

De Gouw, J. and Jimenez, J. L.: Organic Aerosols in the Earth's Atmosphere, Environ. Sci. Technol., 43, 7614-7618, 2009, 10.1021/es9006004.

de Gouw, J. A., Middlebrook, A. M., Warneke, C., Goldan, P. D., Kuster, W. C., Roberts, J. M., Fehsenfeld, F. C., Worsnop, D. R., Canagaratna, M. R., Pszenny, A. A. P., Keene, W. C., Marchewka, M., Bertman, S. B., and Bates, T. S.: Budget of organic carbon in a polluted atmosphere: Results from the New England Air Quality Study in 2002, J. Geophys. Res. Atmos., 110, D16305, 2005, 10.1029/2004JD005623.

de Gouw, J. A., Brock, C. A., Atlas, E. L., Bates, T. S., Fehsenfeld, F. C., Goldan, P. D., Holloway, J. S., Kuster, W. C., Lerner, B. M., Matthew, B. M., Middlebrook, A. M., Onasch, T. B., Peltier, R. E., Quinn, P. K., Senff, C. J., Stohl, A., Sullivan, A. P., Trainer, M., Warneke, C., Weber, R. J., and Williams, E. J.: Sources of particulate matter in the northeastern United States in summer: 1. Direct emissions and secondary formation of organic matter in urban plumes, J. Geophys. Res. Atmos., 113, D08301, 2008, 10.1029/2007JD009243.

de Sá, S. S., Palm, B. B., Campuzano-Jost, P., Day, D. A., Newburn, M. K., Hu, W., Isaacman-VanWertz, G., Yee, L. D., Thalman, R., Brito, J., Carbone, S., Artaxo, P., Goldstein, A. H., Manzi, A. O., Souza, R. A. F., Mei, F., Shilling, J. E., Springston, S. R., Wang, J., Surratt, J. D., Alexander, M. L., Jimenez, J. L., and Martin, S. T.: Influence of urban pollution on the production of organic particulate matter from isoprene epoxydiols in central Amazonia, Atmos. Chem. Phys., 17, 6611-6629, 2017, 10.5194/acp-17-6611-2017.

de Sá, S. S., Wernis, R., Palm, B. B., Yee, L. D., Isaacman-vanWertz, G., and Martin, S. T., in preparation.

DeCarlo, P. F., Kimmel, J. R., Trimborn, A., Northway, M. J., Jayne, J. T., Aiken, A. C., Gonin, M., Fuhrer, K., Horvath, T., Docherty, K. S., Worsnop, D. R., and Jimenez, J. L.: Field-deployable, high-resolution, time-of-flight aerosol mass spectrometer, Anal. Chem., 78, 8281-8289, 2006, 10.1021/ac061249n.

dos Santos, M. J., Silva Dias, M. A. F., and Freitas, E. D.: Influence of local circulations on wind, moisture, and precipitation close to Manaus City, Amazon Region, Brazil, J. Geophys. Res. Atmos., 119, 13,233-213,249, 2014, 10.1002/2014JD021969.

Draxler, R. and Hess, G.: An overview of the HYSPLIT_4 modeling system for trajectories, dispersion, and deposition, Aust. Met. Mag., 47, 295-308, 1998.

Ervens, B., Turpin, B., and Weber, R.: Secondary organic aerosol formation in cloud droplets and aqueous particles (aqSOA): a review of laboratory, field and model studies, Atmos. Chem. Phys., 11, 11069-11102, 2011, 10.5194/acp-11-11069-2011.

Farmer, D. K., Matsunaga, A., Docherty, K. S., Surratt, J. D., Seinfeld, J. H., Ziemann, P. J., and Jimenez, J. L.: Response of an aerosol mass spectrometer to organonitrates and organosulfates and implications for atmospheric chemistry, Proc. Natl. Acad. Sci. USA, 107, 6670-6675, 2010, 10.1073/pnas.0912340107.

Fry, J. L., Kiendler-Scharr, A., Rollins, A. W., Wooldridge, P. J., Brown, S. S., Fuchs, H., Dubé, W., Mensah, A., dal Maso, M., Tillmann, R., Dorn, H. P., Brauers, T., and Cohen, R. C.: Organic nitrate and secondary organic aerosol yield from NO<sub>3</sub> oxidation of β-pinene evaluated using a gas-phase kinetics/aerosol partitioning model, Atmos. Chem. Phys., 9, 1431-1449, 2009, 10.5194/acp-9-1431-2009.

Fry, J. L., Draper, D. C., Zarzana, K. J., Campuzano-Jost, P., Day, D. A., Jimenez, J. L., Brown, S. S., Cohen, R. C., Kaser, L., Hansel, A., Cappellin, L., Karl, T., Hodzic Roux, A.,

Turnipseed, A., Cantrell, C., Lefer, B. L., and Grossberg, N.: Observations of gas- and aerosol-phase organic nitrates at BEACHON-RoMBAS 2011, Atmos. Chem. Phys., 13, 8585-8605, 2013, 10.5194/acp-13-8585-2013.

Glasius, M. and Goldstein, A. H.: Recent discoveries and future challenges in atmospheric organic chemistry, Environ. Sci. Technol., 50, 2754-2764, 2016, 10.1021/acs.est.5b05105.

Goldstein, A. H., Koven, C. D., Heald, C. L., and Fung, I. Y.: Biogenic carbon and anthropogenic pollutants combine to form a cooling haze over the southeastern United States, Proc. Natl Acad. Sci. USA, 106, 8835-8840, 2009, 10.1073/pnas.0904128106.

Guenther, A., Jiang, X., Heald, C., Sakulyanontvittaya, T., Duhl, T., Emmons, L., and Wang, X.: The Model of Emissions of Gases and Aerosols from Nature version 2.1 (MEGAN2. 1): an extended and updated framework for modeling biogenic emissions, Geosci. Model Dev., 5, 1471–1492, 2012, 10.5194/gmd-5-1471-2012.

Hallquist, M., Wenger, J. C., Baltensperger, U., Rudich, Y., Simpson, D., Claeys, M., Dommen, J., Donahue, N. M., George, C., Goldstein, A. H., Hamilton, J. F., Herrmann, H., Hoffmann, T., Iinuma, Y., Jang, M., Jenkin, M. E., Jimenez, J. L., Kiendler-Scharr, A., Maenhaut, W., McFiggans, G., Mentel, T. F., Monod, A., Prévôt, A. S. H., Seinfeld, J. H., Surratt, J. D., Szmigielski, R., and Wildt, J.: The formation, properties and impact of secondary organic aerosol: current and emerging issues, Atmos. Chem. Phys., 9, 5155-5236, 2009, 10.5194/acp-9-5155-2009.

Heald, C. L., Coe, H., Jimenez, J. L., Weber, R. J., Bahreini, R., Middlebrook, A. M., Russell, L. M., Jolleys, M., Fu, T. M., Allan, J. D., Bower, K. N., Capes, G., Crosier, J., Morgan, W. T., Robinson, N. H., Williams, P. I., Cubison, M. J., DeCarlo, P. F., and Dunlea, E. J.: Exploring the vertical profile of atmospheric organic aerosol: comparing 17 aircraft field campaigns with a global model, Atmos. Chem. Phys., 11, 12673-12696, 2011, 10.5194/acp-11-12673-2011.

Hou, A. Y., Kakar, R. K., Neeck, S., Azarbarzin, A. A., Kummerow, C. D., Kojima, M., Oki, R., Nakamura, K., and Iguchi, T.: The Global Precipitation Measurement mission, Bull. Am. Meteorol. Soc., 95, 701-722, 2014, 10.1175/bams-d-13-00164.1.

Hoyle, C. R., Myhre, G., Berntsen, T. K., and Isaksen, I. S. A.: Anthropogenic influence on SOA and the resulting radiative forcing, Atmos. Chem. Phys., 9, 2715-2728, 2009, 10.5194/acp-9-2715-2009.

Hoyle, C. R., Boy, M., Donahue, N. M., Fry, J. L., Glasius, M., Guenther, A., Hallar, A. G., Huff Hartz, K., Petters, M. D., Petäjä, T., Rosenoern, T., and Sullivan, A. P.: A review of the anthropogenic influence on biogenic secondary organic aerosol, Atmos. Chem. Phys., 11, 321-343, 2011, 10.5194/acp-11-321-2011.

Hu, W., Hu, M., Hu, W., Jimenez, J. L., Yuan, B., Chen, W., Wang, M., Wu, Y., Chen, C., Wang, Z., Peng, J., Zeng, L., and Shao, M.: Chemical composition, sources, and aging process of submicron aerosols in Beijing: Contrast between summer and winter, J. Geophys. Res. Atmos., 121, 1955-1977, 2016, 10.1002/2015JD024020.

Hu, W. W., Campuzano-Jost, P., Palm, B. B., Day, D. A., Ortega, A. M., Hayes, P. L., Krechmer, J. E., Chen, Q., Kuwata, M., Liu, Y. J., de Sá, S. S., McKinney, K., Martin, S. T., Hu, M., Budisulistiorini, S. H., Riva, M., Surratt, J. D., St. Clair, J. M., Isaacman-Van Wertz, G., Yee, L. D., Goldstein, A. H., Carbone, S., Brito, J., Artaxo, P., de Gouw, J. A., Koss, A., Wisthaler, A., Mikoviny, T., Karl, T., Kaser, L., Jud, W., Hansel, A., Docherty, K. S., Alexander, M. L., Robinson, N. H., Coe, H., Allan, J. D., Canagaratna, M. R.,

Paulot, F., and Jimenez, J. L.: Characterization of a real-time tracer for isoprene epoxydiols-derived secondary organic aerosol (IEPOX-SOA) from aerosol mass spectrometer measurements, Atmos. Chem. Phys., 15, 11807-11833, 2015, 10.5194/acp-15-11807-2015.

Huang, R.-J., Zhang, Y., Bozzetti, C., Ho, K.-F., Cao, J.-J., Han, Y., Daellenbach, K. R., Slowik, J. G., Platt, S. M., Canonaco, F., Zotter, P., Wolf, R., Pieber, S. M., Bruns, E. A., Crippa, M., Ciarelli, G., Piazzalunga, A., Schwikowski, M., Abbaszade, G., Schnelle-Kreis, J., Zimmermann, R., An, Z., Szidat, S., Baltensperger, U., Haddad, I. E., and Prevot, A. S. H.: High secondary aerosol contribution to particulate pollution during haze events in China, Nature, 514, 218-222, 2014, 10.1038/nature13774.

Isaacman-VanWertz, G., Yee, L. D., Kreisberg, N. M., Wernis, R., Moss, J. A., Hering, S. V., de Sá, S. S., Martin, S. T., Alexander, M. L., Palm, B. B., Hu, W., Campuzano-Jost, P., Day, D. A., Jimenez, J. L., Riva, M., Surratt, J. D., Viegas, J., Manzi, A., Edgerton, E., Baumann, K., Souza, R., Artaxo, P., and Goldstein, A. H.: Ambient Gas-Particle Partitioning of Tracers for Biogenic Oxidation, Environ. Sci. Technol., 9952-9962, 2016, 10.1021/acs.est.6b01674.

Jimenez, J. L., Canagaratna, M. R., Donahue, N. M., Prevot, A. S. H., Zhang, Q., Kroll, J. H., DeCarlo, P. F., Allan, J. D., Coe, H., Ng, N. L., Aiken, A. C., Docherty, K. S., Ulbrich, I. M., Grieshop, A. P., Robinson, A. L., Duplissy, J., Smith, J. D., Wilson, K. R., Lanz, V. A., Hueglin, C., Sun, Y. L., Tian, J., Laaksonen, A., Raatikainen, T., Rautiainen, J., Vaattovaara, P., Ehn, M., Kulmala, M., Tomlinson, J. M., Collins, D. R., Cubison, M. J., Dunlea, J., Huffman, J. A., Onasch, T. B., Alfarra, M. R., Williams, P. I., Bower, K., Kondo, Y., Schneider, J., Drewnick, F., Borrmann, S., Weimer, S., Demerjian, K., Salcedo, D., Cottrell, L., Griffin, R., Takami, A., Miyoshi, T., Hatakeyama, S., Shimono, A., Sun, J. Y., Zhang, Y. M., Dzepina, K., Kimmel, J. R., Sueper, D., Jayne, J. T., Herndon, S. C., Trimborn, A. M., Williams, L. R., Wood, E. C., Middlebrook, A. M., Kolb, C. E., Baltensperger, U., and Worsnop, D. R.: Evolution of organic aerosols in the atmosphere, Science, 326, 1525-1529, 2009, 10.1126/science.1180353.

Joss, J. and Waldvogel, A.: Ein Spektrograph für Niederschlagstropfen mit automatischer Auswertung, Pure and Applied Geophysics, 68, 240-246, 1967, 10.1007/BF00874898.

Krechmer, J. E., Coggon, M. M., Massoli, P., Nguyen, T. B., Crounse, J. D., Hu, W., Day, D. A., Tyndall, G. S., Henze, D. K., Rivera-Rios, J. C., Nowak, J. B., Kimmel, J. R., Mauldin, R. L., Stark, H., Jayne, J. T., Sipilä, M., Junninen, H., Clair, J. M. S., Zhang, X., Feiner, P. A., Zhang, L., Miller, D. O., Brune, W. H., Keutsch, F. N., Wennberg, P. O., Seinfeld, J. H., Worsnop, D. R., Jimenez, J. L., and Canagaratna, M. R.: Formation of low volatility organic compounds and secondary organic aerosol from isoprene hydroxyhydroperoxide low-NO oxidation, Environ. Sci. Technol., 49, 10330-10339, 2015, 10.1021/acs.est.5b02031.

Kroll, J. H., Ng, N. L., Murphy, S. M., Flagan, R. C., and Seinfeld, J. H.: Secondary organic aerosol formation from isoprene photooxidation under high-$NO_x$ conditions, Geophys. Res. Lett., 32, 2005, 10.1029/2005GL023637.

Kroll, J. H., Ng, N. L., Murphy, S. M., Flagan, R. C., and Seinfeld, J. H.: Secondary organic aerosol formation from isoprene photooxidation, Environ. Sci. Technol., 40, 1869-1877, 2006, 10.1021/es0524301.

Kuhn, U., Ganzeveld, L., Thielmann, A., Dindorf, T., Schebeske, G., Welling, M., Sciare, J., Roberts, G., Meixner, F. X., Kesselmeier, J., Lelieveld, J., Kolle, O., Ciccioli, P., Lloyd,

J., Trentmann, J., Artaxo, P., and Andreae, M. O.: Impact of Manaus City on the Amazon Green Ocean atmosphere: ozone production, precursor sensitivity and aerosol load, Atmos. Chem. Phys., 10, 9251-9282, 2010, 10.5194/acp-10-9251-2010.

Kummerow, C., Barnes, W., Kozu, T., Shiue, J., and Simpson, J.: The Tropical Rainfall Measuring Mission (TRMM) sensor package, J. Atmos. Ocea. Technol., 15, 809-817, 1998, 10.1175/1520-0426(1998)015<0809:ttrmmt>2.0.co;2.

Kuwata, M., Liu, Y., McKinney, K., and Martin, S. T.: Physical state and acidity of inorganic sulfate can regulate the production of secondary organic material from isoprene photooxidation products, Phys. Chem. Chem. Phys., 17, 5670-5678, 2015, 10.1039/C4CP04942J.

Lack, D. A., Cappa, C. D., Covert, D. S., Baynard, T., Massoli, P., Sierau, B., Bates, T. S., Quinn, P. K., Lovejoy, E. R., and Ravishankara, A. R.: Bias in filter-based aerosol light absorption measurements due to organic aerosol loading: evidence from ambient measurements, Aerosol Sci Technol, 42, 1033-1041, 2008, 10.1080/02786820802389277.

Lambe, A. T., Onasch, T. B., Massoli, P., Croasdale, D. R., Wright, J. P., Ahern, A. T., Williams, L. R., Worsnop, D. R., Brune, W. H., and Davidovits, P.: Laboratory studies of the chemical composition and cloud condensation nuclei (CCN) activity of secondary organic aerosol (SOA) and oxidized primary organic aerosol (OPOA), Atmos. Chem. Phys., 11, 8913-8928, 2011, 10.5194/acp-11-8913-2011.

Lanz, V. A., Alfarra, M. R., Baltensperger, U., Buchmann, B., Hueglin, C., and Prévôt, A. S. H.: Source apportionment of submicron organic aerosols at an urban site by factor analytical modelling of aerosol mass spectra, Atmos. Chem. Phys., 7, 1503-1522, 2007, 10.5194/acp-7-1503-2007.

Li, Y. J., Liu, P., Gong, Z., Wang, Y., Bateman, A. P., Bergoend, C., Bertram, A. K., and Martin, S. T.: Chemical reactivity and liquid/nonliquid states of secondary organic material, Environ. Sci. Technol., 49, 13264-13274, 2015, 10.1021/acs.est.5b03392.

Liao, J., Froyd, K. D., Murphy, D. M., Keutsch, F. N., Yu, G., Wennberg, P. O., St. Clair, J. M., Crounse, J. D., Wisthaler, A., Mikoviny, T., Jimenez, J. L., Campuzano-Jost, P., Day, D. A., Hu, W., Ryerson, T. B., Pollack, I. B., Peischl, J., Anderson, B. E., Ziemba, L. D., Blake, D. R., Meinardi, S., and Diskin, G.: Airborne measurements of organosulfates over the continental US, J. Geophys. Res. Atmos., 120, 2990-3005, 2015, 10.1002/2014JD022378.

Lin, Y.-H., Zhang, Z., Docherty, K. S., Zhang, H., Budisulistiorini, S. H., Rubitschun, C. L., Shaw, S. L., Knipping, E. M., Edgerton, E. S., Kleindienst, T. E., Gold, A., and Surratt, J. D.: Isoprene epoxydiols as precursors to secondary organic aerosol formation: acid-catalyzed reactive uptake studies with authentic compounds, Environ. Sci. Technol., 46, 250-258, 2012, 10.1021/es202554c.

Liu, J., D'Ambro, E. L., Lee, B. H., Lopez-Hilfiker, F. D., Zaveri, R. A., Rivera-Rios, J. C., Keutsch, F. N., Iyer, S., Kurten, T., Zhang, Z., Gold, A., Surratt, J. D., Shilling, J. E., and Thornton, J. A.: Efficient isoprene secondary organic aerosol formation from a non-IEPOX pathway, Environ. Sci. Technol., 2016a, 10.1021/acs.est.6b01872.

Liu, P., Li, Y. J., Wang, Y., Bateman, A. P., Zhang, Y., Gong, Z., Bertram, A. K., and Martin, S. T.: Highly viscous states affect the browning of atmospheric organic particulate matter, ACS Cent Sci, 2018, 10.1021/acscentsci.7b00452.

Liu, Y., Brito, J., Dorris, M. R., Rivera-Rios, J. C., Seco, R., Bates, K. H., Artaxo, P., Duvoisin, S., Keutsch, F. N., Kim, S., Goldstein, A. H., Guenther, A. B., Manzi, A. O., Souza, R. A. F., Springston, S. R., Watson, T. B., McKinney, K. A., and Martin, S. T.: Isoprene photochemistry over the Amazon rain forest, Proc. Natl. Acad. Sci. USA, 113, 6125-6130, 2016b, 10.1073/pnas.1524136113.

Liu, Y., Seco, R., Kim, S., Guenther, A. B., Goldstein, A. H., Keutsch, F. N., Springston, S. R., Watson, T. B., Artaxo, P., Souza, R. A. F., McKinney, K. A., and Martin, S. T.: Isoprene photo-oxidation products quantify the effect of pollution on hydroxyl radicals over Amazonia, Science Advances, accepted.

Machado, L. A. T., Dias, M. A. F. S., Morales, C., Fisch, G., Vila, D., Albrecht, R., Goodman, S. J., Calheiros, A. J. P., Biscaro, T., Kummerow, C., Cohen, J., Fitzjarrald, D., Nascimento, E. L., Sakamoto, M. S., Cunningham, C., Chaboureau, J.-P., Petersen, W. A., Adams, D. K., Baldini, L., Angelis, C. F., Sapucci, L. F., Salio, P., Barbosa, H. M. J., Landulfo, E., Souza, R. A. F., Blakeslee, R. J., Bailey, J., Freitas, S., Lima, W. F. A., and Tokay, A.: The Chuva Project: how does convection vary across Brazil?, Bull. Am. Meteorol. Soc., 95, 1365-1380, 2014, 10.1175/bams-d-13-00084.1.

Martin, S. T., Andreae, M. O., Artaxo, P., Baumgardner, D., Chen, Q., Goldstein, A. H., Guenther, A., Heald, C. L., Mayol-Bracero, O. L., McMurry, P. H., Pauliquevis, T., Pöschl, U., Prather, K. A., Roberts, G. C., Saleska, S. R., Silva Dias, M. A., Spracklen, D. V., Swietlicki, E., and Trebs, I.: Sources and properties of Amazonian aerosol particles, Rev. Geophys., 48, RG2012, 2010a, 10.1029/2008RG000280.

Martin, S. T., Andreae, M. O., Althausen, D., Artaxo, P., Baars, H., Borrmann, S., Chen, Q., Farmer, D. K., Guenther, A., Gunthe, S. S., Jimenez, J. L., Karl, T., Longo, K., Manzi, A., Müller, T., Pauliquevis, T., Petters, M. D., Prenni, A. J., Pöschl, U., Rizzo, L. V., Schneider, J., Smith, J. N., Swietlicki, E., Tota, J., Wang, J., Wiedensohler, A., and Zorn, S. R.: An overview of the Amazonian aerosol characterization experiment 2008 (AMAZE-08), Atmos. Chem. Phys., 10, 11415-11438, 2010b, 10.5194/acp-10-11415-2010.

Martin, S. T., Artaxo, P., Machado, L. A. T., Manzi, A. O., Souza, R. A. F., Schumacher, C., Wang, J., Andreae, M. O., Barbosa, H. M. J., Fan, J., Fisch, G., Goldstein, A. H., Guenther, A., Jimenez, J. L., Pöschl, U., Silva Dias, M. A., Smith, J. N., and Wendisch, M.: Introduction: observations and modeling of the green ocean Amazon (GoAmazon2014/5), Atmos. Chem. Phys., 16, 4785-4797, 2016, 10.5194/acp-16-4785-2016.

Martin, S. T., Artaxo, P., Machado, L., Manzi, A. O., Souza, R. A. F., Schumacher, C., Wang, J., Biscaro, T., Brito, J., Calheiros, A., Jardine, K., Medeiros, A., Portela, B., Sá, S. S. d., Adachi, K., Aiken, A. C., Albrecht, R., Alexander, L., Andreae, M. O., Barbosa, H. M. J., Buseck, P., Chand, D., Comstock, J. M., Day, D. A., Dubey, M., Fan, J., Fast, J., Fisch, G., Fortner, E., Giangrande, S., Gilles, M., Goldstein, A. H., Guenther, A., Hubbe, J., Jensen, M., Jimenez, J. L., Keutsch, F. N., Kim, S., Kuang, C., Laskin, A., McKinney, K., Mei, F., Miller, M., Nascimento, R., Pauliquevis, T., Pekour, M., Peres, J., Petäjä, T., Pöhlker, C., Pöschl, U., Rizzo, L., Schmid, B., Shilling, J. E., Dias, M. A. S., Smith, J. N., Tomlinson, J. M., Tóta, J., and Wendisch, M.: The Green Ocean Amazon Experiment (GoAmazon2014/5) observes pollution affecting gases, aerosols, clouds, and rainfall over the rain forest, Bulletin of the American Meteorological Society, 98, 981-997, 2017, 10.1175/bams-d-15-00221.1.

Medeiros, A. S. S., Calderaro, G., Guimarães, P. C., Magalhaes, M. R., Morais, M. V. B., Rafee, S. A. A., Ribeiro, I. O., Andreoli, R. V., Martins, J. A., Martins, L. D., Martin, S. T., and Souza, R. A. F.: Power plant fuel switching and air quality in a tropical, forested environment, Atmos. Chem. Phys., 17, 8987-8998, 2017, 10.5194/acp-17-8987-2017.

Mohr, C., DeCarlo, P. F., Heringa, M. F., Chirico, R., Slowik, J. G., Richter, R., Reche, C., Alastuey, A., Querol, X., Seco, R., Peñuelas, J., Jiménez, J. L., Crippa, M., Zimmermann, R., Baltensperger, U., and Prévôt, A. S. H.: Identification and quantification of organic aerosol from cooking and other sources in Barcelona using aerosol mass spectrometer data, Atmos. Chem. Phys., 12, 1649-1665, 2012, 10.5194/acp-12-1649-2012.

Ng, N., Canagaratna, M., Jimenez, J., Chhabra, P., Seinfeld, J., and Worsnop, D.: Changes in organic aerosol composition with aging inferred from aerosol mass spectra, Atmos. Chem. Phys., 11, 6465-6474, 2011a, 10.5194/acp-11-6465-2011.

Ng, N. L., Canagaratna, M. R., Jimenez, J. L., Zhang, Q., Ulbrich, I. M., and Worsnop, D. R.: Real-time methods for estimating organic component mass concentrations from aerosol mass spectrometer data, Environ. Sci. Technol., 45, 910-916, 2011b, 10.1021/es102951k.

Nguyen, T. B., Coggon, M. M., Bates, K. H., Zhang, X., Schwantes, R. H., Schilling, K. A., Loza, C. L., Flagan, R. C., Wennberg, P. O., and Seinfeld, J. H.: Organic aerosol formation from the reactive uptake of isoprene epoxydiols (IEPOX) onto non-acidified inorganic seeds, Atmos. Chem. Phys., 14, 3497-3510, 2014, 10.5194/acp-14-3497-2014.

Nordin, E. Z., Eriksson, A. C., Roldin, P., Nilsson, P. T., Carlsson, J. E., Kajos, M. K., Hellén, H., Wittbom, C., Rissler, J., Löndahl, J., Swietlicki, E., Svenningsson, B., Bohgard, M., Kulmala, M., Hallquist, M., and Pagels, J. H.: Secondary organic aerosol formation from idling gasoline passenger vehicle emissions investigated in a smog chamber, Atmos. Chem. Phys., 13, 6101-6116, 2013, 10.5194/acp-13-6101-2013.

Odum, J. R., Hoffmann, T., Bowman, F., Collins, D., Flagan, R. C., and Seinfeld, J. H.: Gas/particle partitioning and secondary organic aerosol yields, Environ. Sci. Technol., 30, 2580-2585, 1996, 10.1021/es950943+.

Palm, B. B., de Sá, S. S., Day, D. A., Campuzano-Jost, P., Hu, W., Seco, R., Sjostedt, S. J., Park, J. H., Guenther, A. B., Kim, S., Brito, J., Wurm, F., Artaxo, P., Thalman, R., Wang, J., Yee, L. D., Wernis, R., Isaacman-VanWertz, G., Goldstein, A. H., Liu, Y., Springston, S. R., Souza, R., Newburn, M. K., Alexander, M. L., Martin, S. T., and Jimenez, J. L.: Secondary organic aerosol formation from ambient air in an oxidation flow reactor in central Amazonia, Atmos. Chem. Phys., 18, 467-493, 2018, 10.5194/acp-18-467-2018.

Pankow, J. F.: An absorption model of gas/particle partitioning of organic compounds in the atmosphere, Atmos. Environ., 28, 185-188, 1994, 10.1016/1352-2310(94)90093-0.

Paulot, F., Crounse, J. D., Kjaergaard, H. G., Kürten, A., Clair, J. M. S., Seinfeld, J. H., and Wennberg, P. O.: Unexpected epoxide formation in the gas-phase photooxidation of isoprene, Science, 325, 730-733, 2009, 10.1126/science.1172910.

Perraud, V., Bruns, E. A., Ezell, M. J., Johnson, S. N., Yu, Y., Alexander, M. L., Zelenyuk, A., Imre, D., Chang, W. L., Dabdub, D., Pankow, J. F., and Finlayson-Pitts, B. J.: Nonequilibrium atmospheric secondary organic aerosol formation and growth, Proc. Natl Acad. Sci. USA, 109, 2836-2841, 2012, 10.1073/pnas.1119909109.

Pöhlker, M. L., Ditas, F., Saturno, J., Klimach, T., Hrabě de Angelis, I., Araùjo, A., Brito, J., Carbone, S., Cheng, Y., Chi, X., Ditz, R., Gunthe, S. S., Kandler, K., Kesselmeier, J., Könemann, T., Lavrič, J. V., Martin, S. T., Mikhailov, E., Moran-Zuloaga, D., Rizzo, L. V., Rose, D., Su, H., Thalman, R., Walter, D., Wang, J., Wolff, S., Barbosa, H. M. J.,

Artaxo, P., Andreae, M. O., Pöschl, U., and Pöhlker, C.: Long-term observations of cloud condensation nuclei in the Amazon rain forest – Part 2: Variability and characteristic differences under near-pristine, biomass burning, and long-range transport conditions, Atmos. Chem. Phys. Discuss., 2017, 1-51, 2017, 10.5194/acp-2017-847.

Presto, A. A., Gordon, T. D., and Robinson, A. L.: Primary to secondary organic aerosol: evolution of organic emissions from mobile combustion sources, Atmos. Chem. Phys., 14, 5015-5036, 2014, 10.5194/acp-14-5015-2014.

Riva, M., Budisulistiorini, S. H., Chen, Y., Zhang, Z., D'Ambro, E. L., Zhang, X., Gold, A., Turpin, B. J., Thornton, J. A., Canagaratna, M. R., and Surratt, J. D.: Chemical characterization of secondary organic aerosol from oxidation of isoprene hydroxyhydroperoxides, Environ. Sci. Technol., 2016, 10.1021/acs.est.6b02511.

Robinson, A. L., Donahue, N. M., Shrivastava, M. K., Weitkamp, E. A., Sage, A. M., Grieshop, A. P., Lane, T. E., Pierce, J. R., and Pandis, S. N.: Rethinking organic aerosols: semivolatile emissions and photochemical aging, Science, 315, 1259-1262, 2007, 10.1126/science.1133061.

Robinson, N. H., Hamilton, J. F., Allan, J. D., Langford, B., Oram, D. E., Chen, Q., Docherty, K., Farmer, D. K., Jimenez, J. L., Ward, M. W., Hewitt, C. N., Barley, M. H., Jenkin, M. E., Rickard, A. R., Martin, S. T., McFiggans, G., and Coe, H.: Evidence for a significant proportion of Secondary Organic Aerosol from isoprene above a maritime tropical forest, Atmos. Chem. Phys., 11, 1039-1050, 2011, 10.5194/acp-11-1039-2011.

Röhrl, A. and Lammel, G.: Determination of malic acid and other C4 dicarboxylic acids in atmospheric aerosol samples, Chemosphere, 46, 1195-1199, 2002, doi.org/10.1016/S0045-6535(01)00243-0.

Schneider, J., Weimer, S., Drewnick, F., Borrmann, S., Helas, G., Gwaze, P., Schmid, O., Andreae, M. O., and Kirchner, U.: Mass spectrometric analysis and aerodynamic properties of various types of combustion-related aerosol particles, Int. J. Mass Spectrom., 258, 37-49, 2006, 10.1016/j.ijms.2006.07.008.

Schneider, J., Freutel, F., Zorn, S., Chen, Q., Farmer, D., Jimenez, J., Martin, S., Artaxo, P., Wiedensohler, A., and Borrmann, S.: Mass-spectrometric identification of primary biological particle markers and application to pristine submicron aerosol measurements in Amazonia, Atmos Chem Phys, 11, 11415-11429, 2011, doi.org/10.5194/acp-11-11415-2011.

Setyan, A., Zhang, Q., Merkel, M., Knighton, W. B., Sun, Y., Song, C., Shilling, J. E., Onasch, T. B., Herndon, S. C., Worsnop, D. R., Fast, J. D., Zaveri, R. A., Berg, L. K., Wiedensohler, A., Flowers, B. A., Dubey, M. K., and Subramanian, R.: Characterization of submicron particles influenced by mixed biogenic and anthropogenic emissions using high-resolution aerosol mass spectrometry: results from CARES, Atmos. Chem. Phys., 12, 8131-8156, 2012, 10.5194/acp-12-8131-2012.

Shilling, J. E., Zaveri, R. A., Fast, J. D., Kleinman, L., Alexander, M. L., Canagaratna, M. R., Fortner, E., Hubbe, J. M., Jayne, J. T., Sedlacek, A., Setyan, A., Springston, S., Worsnop, D. R., and Zhang, Q.: Enhanced SOA formation from mixed anthropogenic and biogenic emissions during the CARES campaign, Atmos. Chem. Phys., 13, 2091-2113, 2013, 10.5194/acp-13-2091-2013.

Shilling, J. E., Fortner, E., Pekour, M. S., Artaxo, P., Hubbe, J. M., Longo, K. M., Machado, L. A. T., Martin, S. T., Mei, F., Springston, S. R., Tomlinson, J., and Wang, J.: Particle-

phase chemical composition measurements onboard the G-1 research aircraft during the GoAmazon2014/5 campaign in preparation.
Shrivastava, M., Cappa, C. D., Fan, J., Goldstein, A. H., Guenther, A. B., Jimenez, J. L., Kuang, C., Laskin, A., Martin, S. T., Ng, N. L., Petaja, T., Pierce, J. R., Rasch, P. J., Roldin, P., Seinfeld, J. H., Shilling, J., Smith, J. N., Thornton, J. A., Volkamer, R., Wang, J., Worsnop, D. R., Zaveri, R. A., Zelenyuk, A., and Zhang, Q.: Recent advances in understanding secondary organic aerosol: Implications for global climate forcing, Rev. Geophys., 55, 509-559, 2017, 10.1002/2016RG000540.
Spracklen, D. V., Jimenez, J. L., Carslaw, K. S., Worsnop, D. R., Evans, M. J., Mann, G. W., Zhang, Q., Canagaratna, M. R., Allan, J., Coe, H., McFiggans, G., Rap, A., and Forster, P.: Aerosol mass spectrometer constraint on the global secondary organic aerosol budget, Atmos. Chem. Phys., 11, 12109-12136, 2011, 10.5194/acp-11-12109-2011.
Subramanian, R., Roden, C. A., Boparai, P., and Bond, T. C.: Yellow beads and missing particles: trouble ahead for filter-based absorption measurements, Aerosol Sci Technol, 41, 630-637, 2007, 10.1080/02786820701344589.
Sueper, D. and collaborators: ToF-AMS Data Analysis Software Webpage, http://cires1.colorado.edu/jimenez-group/wiki/index.php/ToF-AMS_Analysis_Software, last access: August 2017.
Surratt, J. D., Chan, A. W., Eddingsaas, N. C., Chan, M., Loza, C. L., Kwan, A. J., Hersey, S. P., Flagan, R. C., Wennberg, P. O., and Seinfeld, J. H.: Reactive intermediates revealed in secondary organic aerosol formation from isoprene, Proc. Natl. Acad. Sci. USA, 107, 6640-6645, 2010, 10.1073/pnas.0911114107.
Thalman, R., de Sá, S. S., Palm, B. B., Barbosa, H. M. J., Pöhlker, M. L., Alexander, M. L., Brito, J., Carbone, S., Castillo, P., Day, D. A., Kuang, C., Manzi, A., Ng, N. L., Sedlacek Iii, A. J., Souza, R., Springston, S., Watson, T., Pöhlker, C., Pöschl, U., Andreae, M. O., Artaxo, P., Jimenez, J. L., Martin, S. T., and Wang, J.: CCN activity and organic hygroscopicity of aerosols downwind of an urban region in central Amazonia: seasonal and diel variations and impact of anthropogenic emissions, Atmos. Chem. Phys., 17, 11779-11801, 2017, 10.5194/acp-17-11779-2017.
Tsigaridis, K., Krol, M., Dentener, F. J., Balkanski, Y., Lathière, J., Metzger, S., Hauglustaine, D. A., and Kanakidou, M.: Change in global aerosol composition since preindustrial times, Atmos. Chem. Phys., 6, 5143-5162, 2006, 10.5194/acp-6-5143-2006.
Ulbrich, I., Handschy, A., Lechner, M. J., and Jimenez, J.: AMS Spectral Database, 2009a, http://cires.colorado.edu/jimenez-group/AMSsd/, last access: August 2017.
Ulbrich, I., Handschy, A., Lechner, M. J., and Jimenez, J.: High-Resolution AMS Spectral Database, 2009b, http://cires.colorado.edu/jimenez-group/HRAMSsd/, last access: August 2017.
Ulbrich, I., Canagaratna, M., Zhang, Q., Worsnop, D., and Jimenez, J.: Interpretation of organic components from positive matrix factorization of aerosol mass spectrometric data, Atmos. Chem. Phys., 9, 2891-2918, 2009c, 10.5194/acp-9-2891-2009.
van Pinxteren, D., Neusüß, C., and Herrmann, H.: On the abundance and source contributions of dicarboxylic acids in size-resolved aerosol particles at continental sites in central Europe, Atmos. Chem. Phys., 14, 3913-3928, 2014.
Weber, R. J., Sullivan, A. P., Peltier, R. E., Russell, A., Yan, B., Zheng, M., de Gouw, J., Warneke, C., Brock, C., Holloway, J. S., Atlas, E. L., and Edgerton, E.: A study of

secondary organic aerosol formation in the anthropogenic-influenced southeastern United States, J. Geophys. Res. Atmos., 112, D13302, 2007, 10.1029/2007JD008408.

Worton, D. R., Surratt, J. D., LaFranchi, B. W., Chan, A. W. H., Zhao, Y., Weber, R. J., Park, J.-H., Gilman, J. B., de Gouw, J., Park, C., Schade, G., Beaver, M., Clair, J. M. S., Crounse, J., Wennberg, P., Wolfe, G. M., Harrold, S., Thornton, J. A., Farmer, D. K., Docherty, K. S., Cubison, M. J., Jimenez, J.-L., Frossard, A. A., Russell, L. M., Kristensen, K., Glasius, M., Mao, J., Ren, X., Brune, W., Browne, E. C., Pusede, S. E., Cohen, R. C., Seinfeld, J. H., and Goldstein, A. H.: Observational insights into aerosol formation from isoprene, Environ. Sci. Technol., 47, 11403-11413, 2013, 10.1021/es4011064.

Xu, L., Guo, H., Boyd, C. M., Klein, M., Bougiatioti, A., Cerully, K. M., Hite, J. R., Isaacman-VanWertz, G., Kreisberg, N. M., Knote, C., Olson, K., Koss, A., Goldstein, A. H., Hering, S. V., de Gouw, J., Baumann, K., Lee, S.-H., Nenes, A., Weber, R. J., and Ng, N. L.: Effects of anthropogenic emissions on aerosol formation from isoprene and monoterpenes in the southeastern United States, Proc. Natl. Acad. Sci. USA, 112, 37-42, 2015a, 10.1073/pnas.1417609112.

Xu, L., Suresh, S., Guo, H., Weber, R. J., and Ng, N. L.: Aerosol characterization over the southeastern United States using high-resolution aerosol mass spectrometry: spatial and seasonal variation of aerosol composition and sources with a focus on organic nitrates, Atmos. Chem. Phys., 15, 7307-7336, 2015b, 10.5194/acp-15-7307-2015.

Yáñez-Serrano, A. M., Nölscher, A. C., Williams, J., Wolff, S., Alves, E., Martins, G. A., Bourtsoukidis, E., Brito, J., Jardine, K., Artaxo, P., and Kesselmeier, J.: Diel and seasonal changes of biogenic volatile organic compounds within and above an Amazonian rainforest, Atmos. Chem. Phys., 15, 3359-3378, 2015, 10.5194/acp-15-3359-2015.

Zhang, H., Yee, L. D., and Goldstein, A. H.: Monoterpenes are the largest source of summertime organic aerosol in the southeastern United States, 2018.

Zhang, Q., Alfarra, M. R., Worsnop, D. R., Allan, J. D., Coe, H., Canagaratna, M. R., and Jimenez, J. L.: Deconvolution and quantification of hydrocarbon-like and oxygenated organic aerosols based on aerosol mass spectrometry, Environ. Sci. Technol., 39, 4938-4952, 2005, 10.1021/es048568l.

Zhang, Q., Jimenez, J. L., Canagaratna, M. R., Ulbrich, I. M., Ng, N. L., Worsnop, D. R., and Sun, Y.: Understanding atmospheric organic aerosols via factor analysis of aerosol mass spectrometry: a review, Anal. Bioanal. Chem., 401, 3045-3067, 2011, 10.1007/s00216-011-5355-y.

**List of Figures**

**Figure 3**. Scatter plot of the AMS signal fraction at *m*/*z* 44 ($f_{44}$) against that at *m*/*z* 43 ($f_{43}$). Gray and blue circles correspond, respectively, to measurements at T3 and T2 during IOP1, in the wet season of 2014. For visualization purposes, the two datasets are plotted separately in panels a and b. Solid squares represent median values, and whiskers represent 10 and 90 percentiles. Dashed lines delineate the region where worldwide measurements of ambient organic $PM_1$ commonly lie (Ng et al., 2011a).

**Figure 4**. Results of the PMF analysis on the time series of AMS organic mass spectra collected at T3. (a) Mass spectral profile of each factor represented at unit mass resolution. The inset shows the mean fractional loading of each factor. (b) Diel trends for the loadings of each PMF factor. Local time is (UTC - 4 h). Lines represent means, solid markers show medians, and boxes span interquartile ranges. (c) Time series of the factor loadings (left axis) and other related measurements at T3 (right axis). Methyl-butyl-tricarboxylic acid is abbreviated as MBTCA.

**Figure 5**. Column plot of Pearson *R* correlations between the loading of each PMF factor and values of selected measurements at T3. Abbreviations include tricarballylic acid (TCA), methyl-butyl-tricarboxylic acid (MBTCA), methyl vinyl ketone (MVK), methacrolein (MACR), and isoprene hydroxyhydroperoxides (ISOPOOH). SV-TAG measurements refer to particle-phase concentrations. Isomers could not be distinguished by PTR-ToF-MS measurements; $C_8$ and $C_9$ aromatics include the xylene and trimethylbenzene isomers, respectively.

**Figure 6**. Results of the cluster analysis by Fuzzy c-means (FCM) for afternoon periods (12:00 to 16:00 h) are presented by several case studies. (a) Degree of membership in each of the four clusters. The sum of degrees of membership across all clusters is unity.

Background conditions are abbreviated as “Bkgd”, and polluted conditions are abbreviated as “Pol”. (b) Pollution indicators: concentrations of $NO_y$, $O_3$, black carbon (BC), and particle number count are plotted. (c) $PM_1$ mass concentrations for organic, sulfate, nitrate, and ammonium species. (d) Fractional contribution of each factor to total organic $PM_1$.

**Figure 7**. Air mass backtrajectories associated with the four clusters of the FCM analysis for the case studies of Figure 6. Trajectories were calculated using HYSPLIT 4 in steps of 12 min for ten hours (Draxler and Hess, 1998). Image data: Google earth.

**Figure 8**. Characteristic PM composition of the FCM clusters as represented by coordinates of cluster centroids. (a) Mass concentrations of AMS species characteristic of each cluster. (b) PMF factor loadings characteristic of each cluster. Calculations are presented in more detail in the Supplementary Material (Section S3). Values plotted are shown in Table 2.

**Figure 9**. Schematic representation of (a) atmospheric processes, illustrated in a simplified manner, associated with the production of organic $PM_1$ and (b) observables of these processes as captured by the datasets and analytical approach employed in this study. In panel (a), the left side depicts the emissions of biogenic volatile organic compounds (VOCs), their atmospheric oxidation, and the production of biogenic secondary organic $PM_1$. The right side depicts anthropogenic emissions of gas species and particulate matter that can alter natural atmospheric concentrations and processes. There are primary organic $PM_1$ emissions from traffic, cooking, and industrial activities. Anthropogenic VOCs can be precursors for the production of secondary organic $PM_1$ and can affect the production of ozone and hydroxyl radical. $NO_x$

emissions directly and indirectly alter the natural pathways of $PM_1$ production in the atmosphere. $NO_x$ and $SO_x$ can also directly contribute to the formation of secondary inorganic $PM_1$ (not shown), which can in turn play a role in changing pathways of secondary organic $PM_1$ production. In panel (b), different PMF factors represent distinct sources and/or processes. The IEPOX-SOA factor is at the intersection of the two, as it represents both a source (i.e., isoprene emissions from the forest) and a process (i.e., photo-oxidation under $HO_2$ dominant conditions, influenced by sulfate concentrations). The dashed black line represents the natural and anthropogenic oxidative processes that transform the chemical signature of the HOA, ADOA, BBOA, IEPOX-SOA, and LO-OOA factors after sufficient atmospheric residence time into the MO-OOA factor. The clusters represent different conditions at the receptor site (i.e., T3) and therefore incorporate the meteorological and geographical histories of the air masses that reach the site and affect the observed concentrations. The different PMF factors are associated to the different clusters (solid lines) to various extents (not detailed here for simplification purposes; cf. Figure 8).

**Table 1.** Characteristics of the PMF factors derived from the AMS datasets. Listed are signal fractions $f_{CO_2^+}$ at nominal $m/z$ 44 and oxygen-to-carbon (O:C) and hydrogen-to-carbon (H:C) ratios. Values and associated uncertainties were calculated by running PMF in "bootstrap mode" (Ulbrich et al., 2009c). Elemental ratios were calibrated by the "improved-ambient" method, which has an estimated uncertainty of 12% for O:C and 4% for H:C (Canagaratna et al., 2015).

| PMF factor | $f_{CO_2^+}$ | O:C | H:C |
|---|---|---|---|
| MO-OOA | 0.25 ± 0.01 | 1.09 ± 0.17 | 1.27 ± 0.12 |
| LO-OOA | 0.14 ± 0.02 | 0.72 ± 0.10 | 1.49 ± 0.07 |
| IEPOX-SOA | 0.17 ± 0.01 | 0.93 ± 0.10 | 1.39 ± 0.07 |
| ADOA | 0.11 ± 0.01 | 0.40 ± 0.05 | 1.63 ± 0.02 |
| BBOA | 0.123 ± 0.004 | 0.61 ± 0.08 | 1.57 ± 0.04 |
| HOA | 0.048 ± 0.006 | 0.18 ± 0.02 | 1.94 ± 0.02 |

**Table 2.** Coordinates of cluster centroids for input variables, AMS species concentrations, and PMF factor loadings. Table entries for AMS species and PMF factors are plotted in Figure 8. The AMS species concentrations (except for sulfate) and PMF factor loadings were not used as input variables in the FCM clustering analysis.

| Species | Cluster Centroid | | | |
|---|---|---|---|---|
| | Bkgd-1 | Bkgd-2 | Pol-1 | Pol-2 |
| Input variables | | | | |
| Particle number ($cm^{-3}$) | 714 | 1117 | 2636 | 6697 |
| $NO_y$ (ppb) | 0.64 | 0.95 | 1.2 | 2.2 |
| $O_3$ (ppb) | 14 | 17 | 26 | 36 |
| Black carbon ($\mu g\ m^{-3}$) | 0.05 | 0.16 | 0.21 | 0.18 |
| Sulfate ($\mu g\ m^{-3}$) | 0.15 | 0.36 | 0.44 | 0.57 |
| AMS species concentrations ($\mu g\ m^{-3}$) | | | | |
| Organic | 0.96 | 2.0 | 2.5 | 2.6 |
| Ammonium | 0.05 | 0.12 | 0.15 | 0.21 |
| Nitrate | 0.03 | 0.07 | 0.10 | 0.12 |
| Chloride | 0.007 | 0.011 | 0.009 | 0.007 |
| PMF factor loadings ($\mu g\ m^{-3}$) | | | | |
| MO-OOA | 0.29 | 0.83 | 1.13 | 1.13 |
| LO-OOA | 0.38 | 0.41 | 0.62 | 0.77 |
| IEPOX-SOA | 0.18 | 0.49 | 0.43 | 0.29 |
| ADOA | 0.044 | 0.086 | 0.19 | 0.32 |
| BBOA | 0.028 | 0.054 | 0.081 | 0.063 |
| HOA | 0.017 | 0.027 | 0.039 | 0.040 |

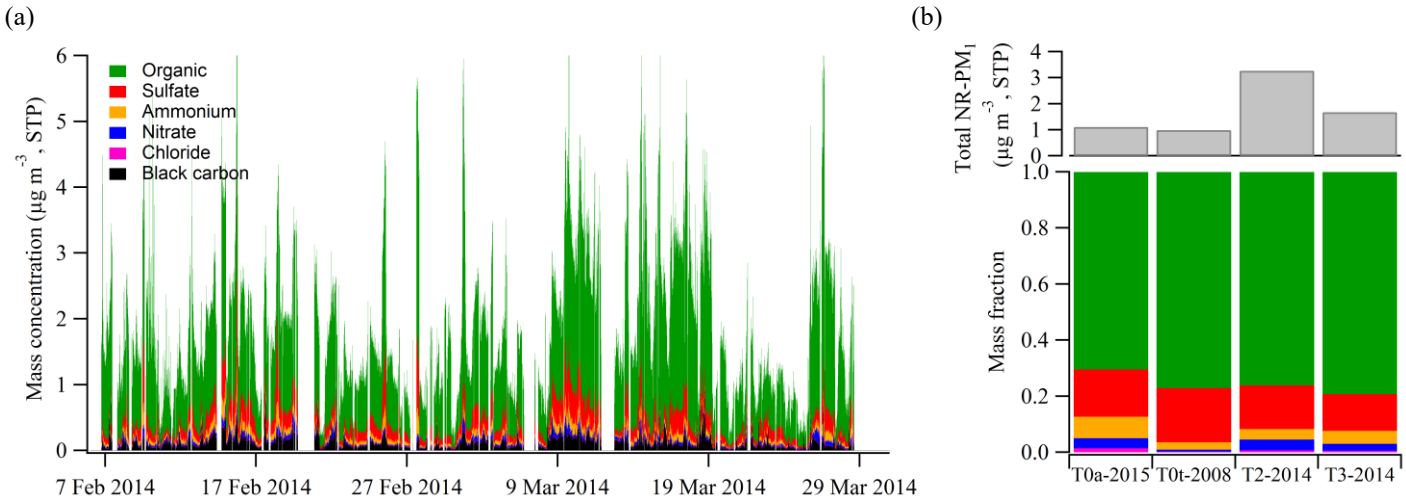
(a)
Organic
Sulfate
Ammonium
Nitrate
Chloride
Black carbon
Mass concentration (µg m-3, STP)
7 Feb 2014
17 Feb 2014
27 Feb 2014
9 Mar 2014
19 Mar 2014
29 Mar 2014
(b)
Total NR-PM1 (µg m-3, STP)
Mass fraction
T0a-2015
T0t-2008
T2-2014
T3-2014

Figure 1

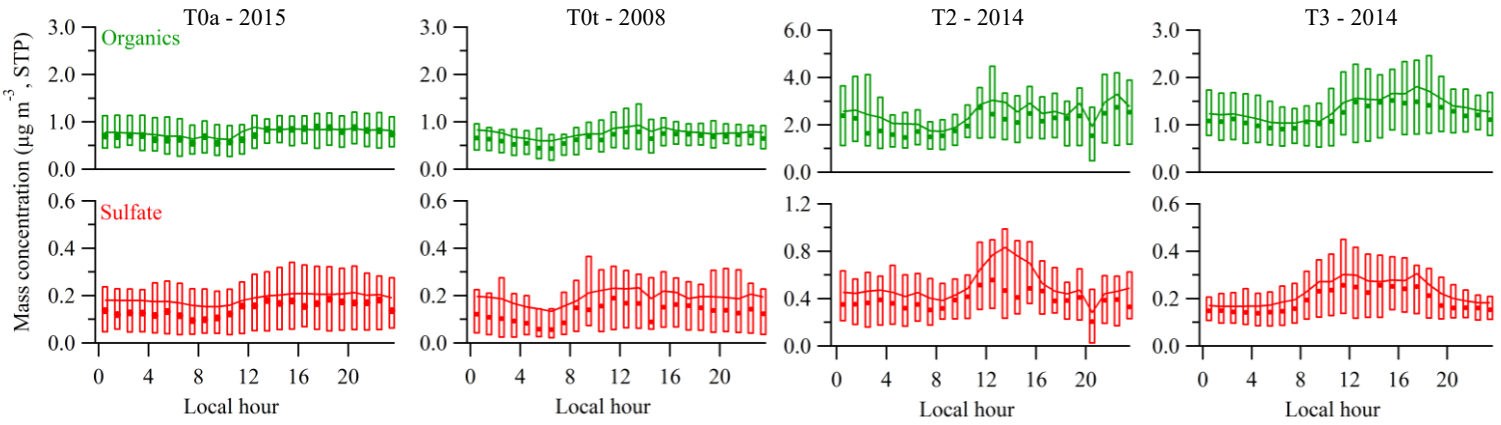
T0a - 2015
T0t - 2008
T2 - 2014
T3 - 2014
Organics
Sulfate
Mass concentration (µg m-3, STP)
Local hour
0
4
8
12
16
20

Figure 2

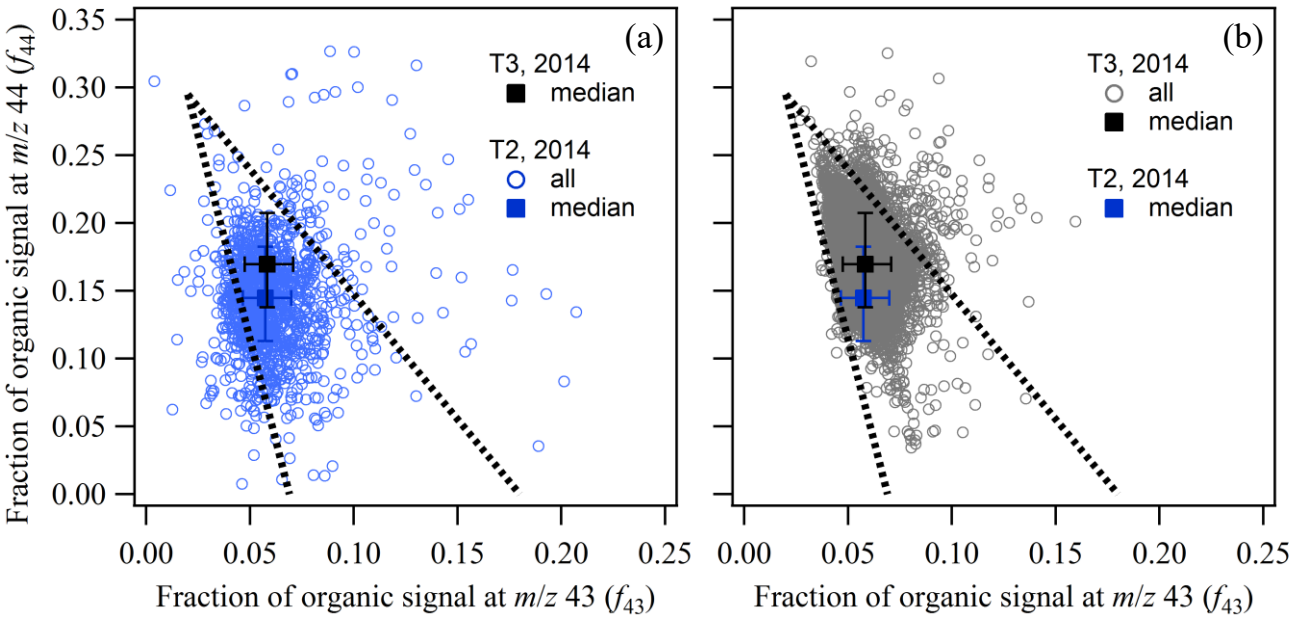
(a)
(b)
T3, 2014
median
T2, 2014
all
median
Fraction of organic signal at m/z 44 ($f_{44}$)
Fraction of organic signal at m/z 43 ($f_{43}$)
0.00
0.05
0.10
0.15
0.20
0.25
0.30
0.35

Figure 3

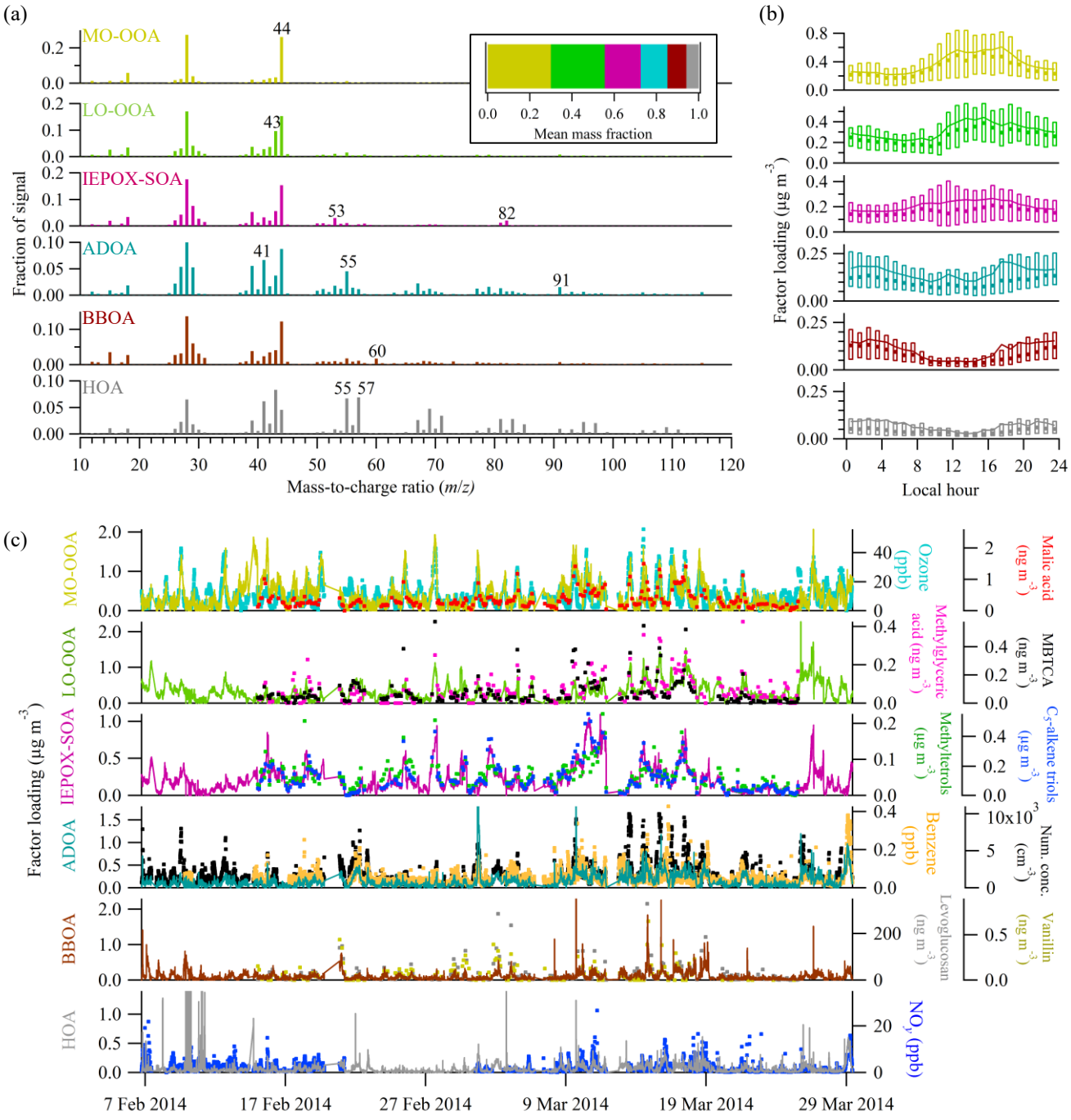
(a)
MO-OOA
LO-OOA
IEPOX-SOA
ADOA
BBOA
HOA
Fraction of signal
Mass-to-charge ratio (m/z)
Mean mass fraction
(b)
Factor loading (μg m-3)
Local hour
(c)
Factor loading (μg m-3)
Ozone (ppb)
Malic acid (ng m-3)
Methylglyceric acid (ng m-3)
MBTCA (ng m-3)
Methyltetrols (μg m-3)
C5-alkene triols (μg m-3)
Benzene (ppb)
Num. conc. (cm-3)
Levoglucosan (ng m-3)
Vanillin (ng m-3)
NOy (ppb)
7 Feb 2014
17 Feb 2014
27 Feb 2014
9 Mar 2014
19 Mar 2014
29 Mar 2014

Figure 4

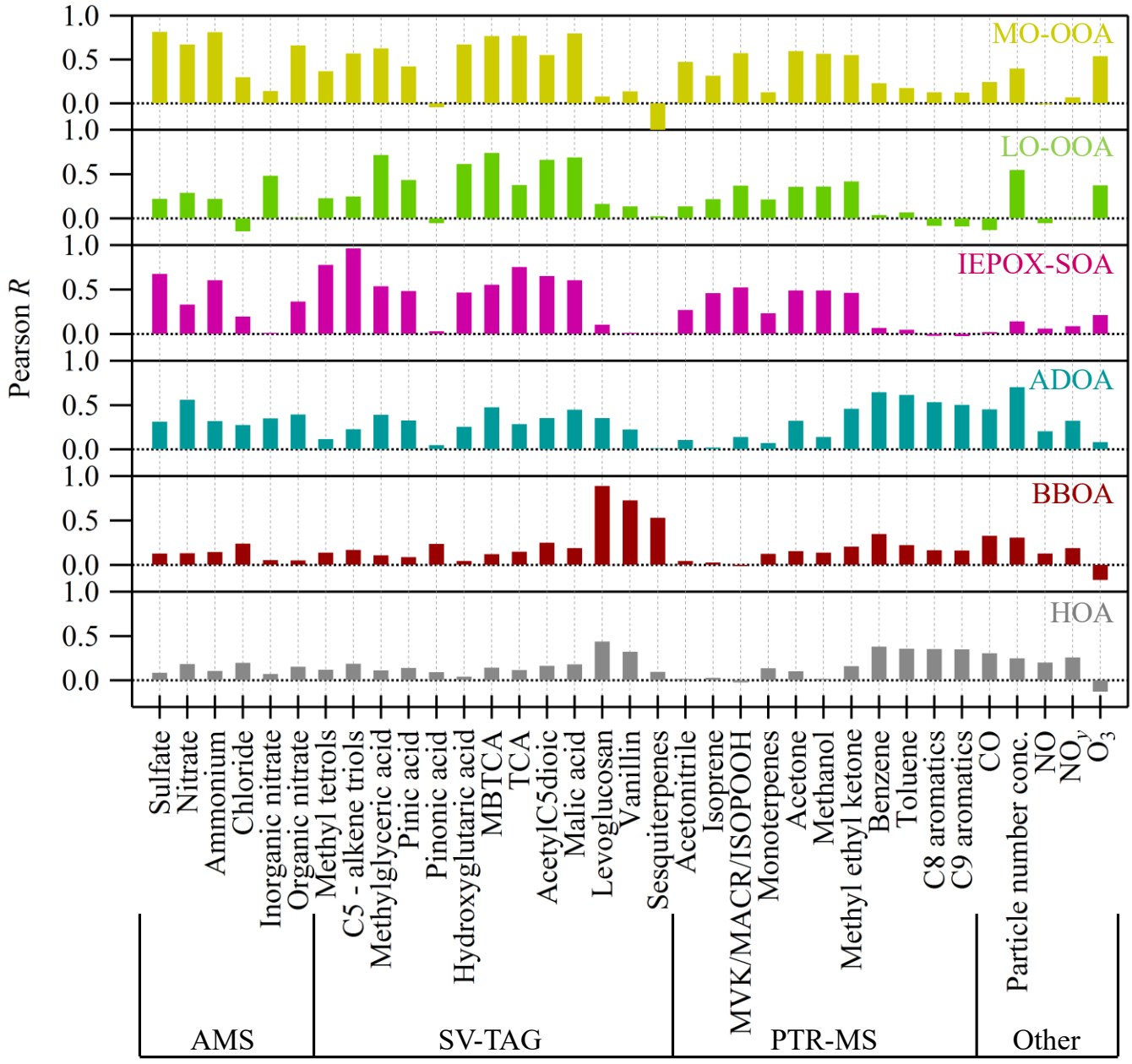
Pearson R
1.0
0.5
0.0
MO-OOA
LO-OOA
IEPOX-SOA
ADOA
BBOA
HOA
Sulfate
Nitrate
Ammonium
Chloride
Inorganic nitrate
Organic nitrate
Methyl tetrols
C5 - alkene triols
Methylglyceric acid
Pinic acid
Pinonic acid
Hydroxyglutaric acid
MBTCA
TCA
AcetylC5dioic
Malic acid
Levoglucosan
Vanillin
Sesquiterpenes
Acetonitrile
Isoprene
MVK/MACR/ISOPOOH
Monoterpenes
Acetone
Methanol
Methyl ethyl ketone
Benzene
Toluene
C8 aromatics
C9 aromatics
CO
Particle number conc.
NO
NOy
O3
AMS
SV-TAG
PTR-MS
Other

Figure 5

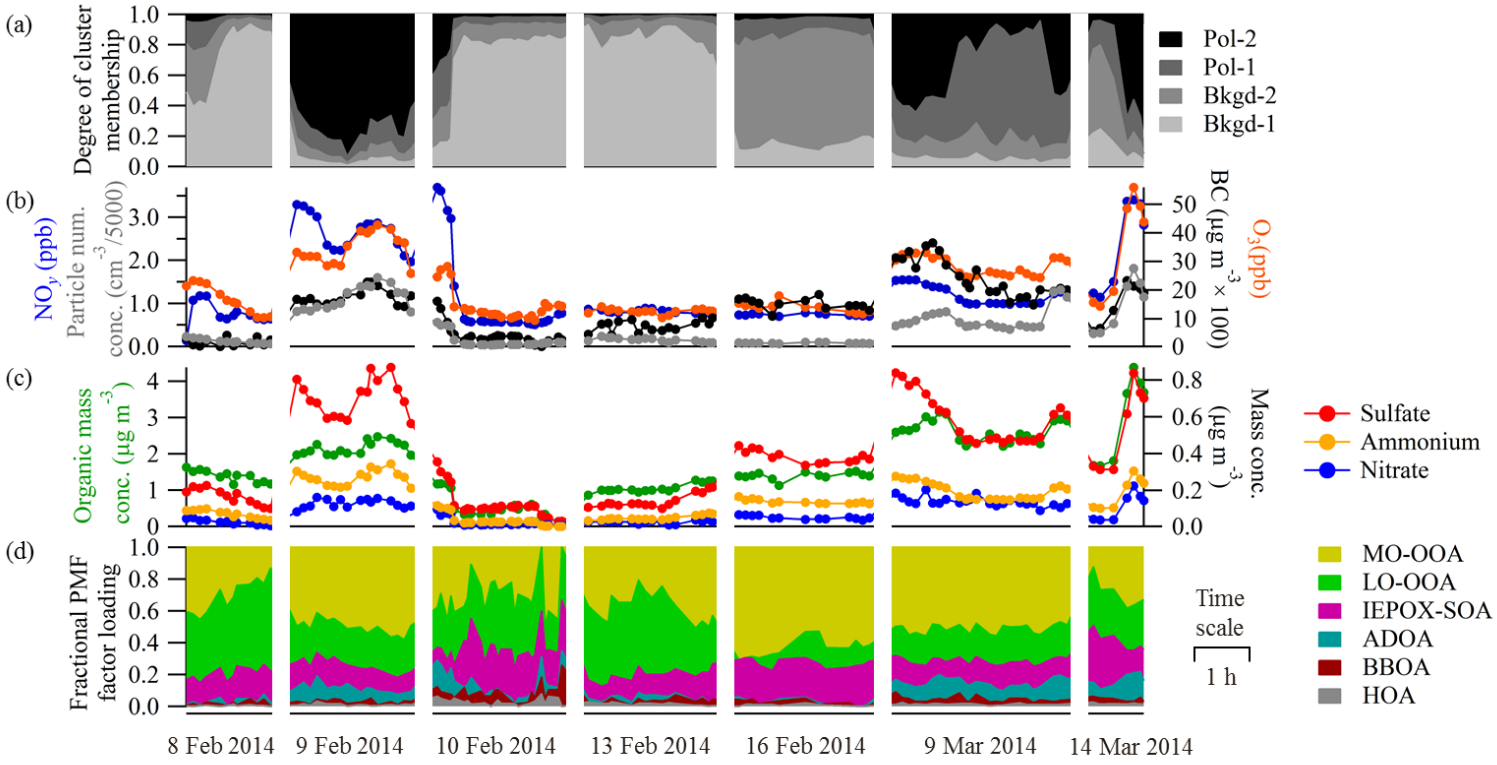
(a)
Degree of cluster membership
1.0
0.8
0.6
0.4
0.2
0.0
Pol-2
Pol-1
Bkgd-2
Bkgd-1
(b)
NOy (ppb)
Particle num. conc. (cm-3/5000)
3.0
2.0
1.0
0.0
BC (μg m-3 × 100)
50
40
30
20
10
0
O3(ppb)
(c)
Organic mass conc. (μg m-3)
4
3
2
1
0
0.8
0.6
0.4
0.2
0.0
Mass conc. (μg m-3)
Sulfate
Ammonium
Nitrate
(d)
Fractional PMF factor loading
1.0
0.8
0.6
0.4
0.2
0.0
Time scale
1 h
MO-OOA
LO-OOA
IEPOX-SOA
ADOA
BBOA
HOA
8 Feb 2014
9 Feb 2014
10 Feb 2014
13 Feb 2014
16 Feb 2014
9 Mar 2014
14 Mar 2014

Figure 6

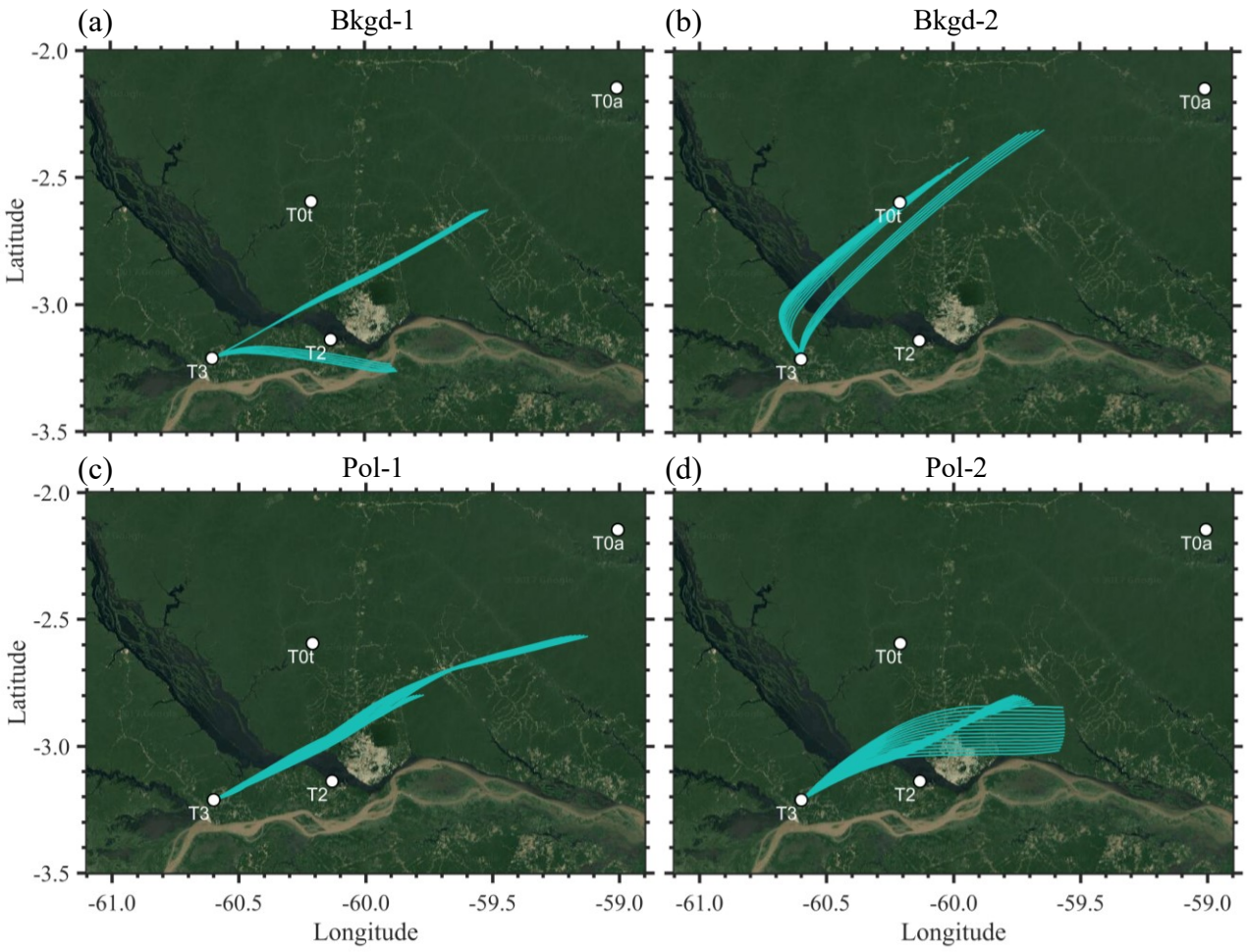
(a)
Bkgd-1
(b)
Bkgd-2
(c)
Pol-1
(d)
Pol-2
T0a
T0t
T2
T3
Latitude
Longitude
-2.0
-2.5
-3.0
-3.5
-61.0
-60.5
-60.0
-59.5
-59.0

Figure 7

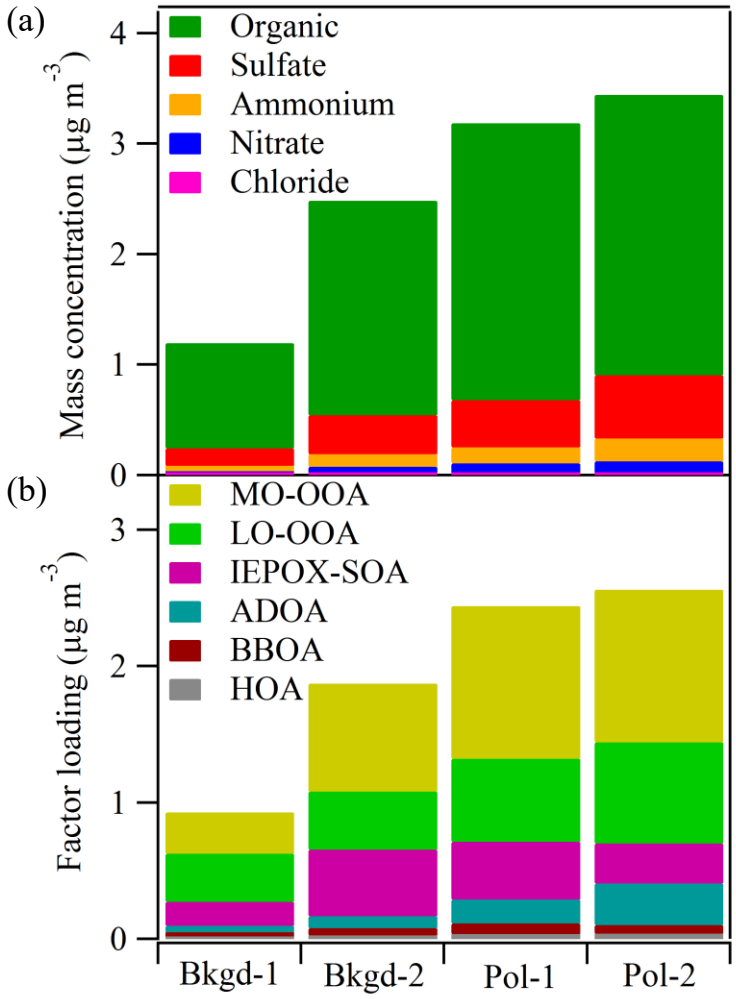
(a)
Organic
Sulfate
Ammonium
Nitrate
Chloride
Mass concentration (µg m-3)
0
1
2
3
4
(b)
MO-OOA
LO-OOA
IEPOX-SOA
ADOA
BBOA
HOA
Factor loading (µg m-3)
0
1
2
3
Bkgd-1
Bkgd-2
Pol-1
Pol-2

*Figure 8*

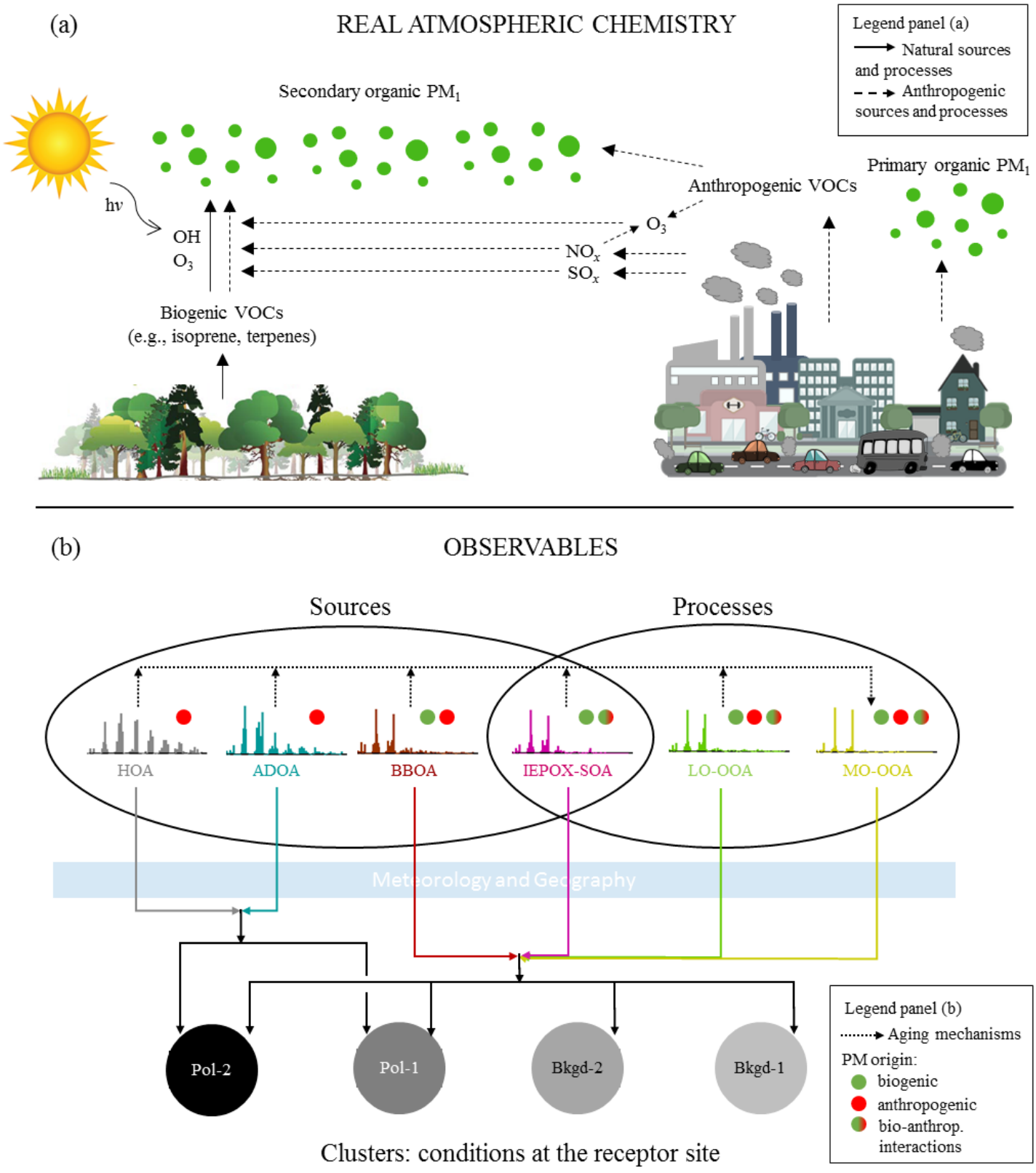
(a)
REAL ATMOSPHERIC CHEMISTRY
Legend panel (a)
Natural sources and processes
Anthropogenic sources and processes
Secondary organic PM1
Primary organic PM1
Anthropogenic VOCs
hν
OH
O3
O3
NOx
SOx
Biogenic VOCs
(e.g., isoprene, terpenes)
(b)
OBSERVABLES
Sources
Processes
HOA
ADOA
BBOA
IEPOX-SOA
LO-OOA
MO-OOA
Meteorology and Geography
Pol-2
Pol-1
Bkgd-2
Bkgd-1
Clusters: conditions at the receptor site
Legend panel (b)
Aging mechanisms
PM origin:
biogenic
anthropogenic
bio-anthrop. interactions

Figure 9